

- the construction of polyplex micelles showing efficient gene transfer toward primary cells. *ChemMedChem* 2006;1:439–44.
- [16] Masago K, Itaka K, Nishiyama N, Chung UI, Kataoka K. Gene delivery with biocompatible cationic polymer: pharmacogenomic analysis on cell bioactivity. *Biomaterials* 2007;28:5169–75.
- [17] Akagi D, Oba M, Koyama H, Nishiyama N, Miyata T, Nagawa H, et al. Biocompatible micellar nanovectors achieve efficient gene transfer to vascular lesions without cytotoxicity and thrombus formation. *J Gene Med* 2008;10: pp. 474–474.
- [18] Itaka K, Ohba S, Miyata K, Kawaguchi H, Nakamura K, Takato T, et al. Bone regeneration by regulated in vivo gene transfer using biocompatible polyplex nanomicelles. *Mol Ther* 2007;15:1655–62.
- [19] Harada-Shiba M, Takamisawa I, Miyata K, Ishii T, Nishiyama N, Itaka K, et al. Intratracheal gene transfer of adrenomedullin using polyplex nanomicelles attenuates monocrotaline-induced pulmonary hypertension in rats. *Mol Ther* 2009;17:1180–6.
- [20] Oba M, Miyata K, Osada K, Christie RJ, Sanjoh M, Li W, et al. Polyplex micelles prepared from  $\omega$ -cholesteryl PEG-polycation block copolymers for systemic gene delivery. *Biomaterials* 2011;32:652–63.
- [21] Kim HJ, Ishii A, Miyata K, Lee Y, Wu S, Oba M, et al. Introduction of stearyl moieties into a biocompatible cationic polyaspartamide derivative, PAsp(-DET), with endosomal escaping function for enhanced siRNA-mediated gene knockdown. *J Control Release* 2010;145:141–8.
- [22] Takemoto H, Ishii A, Miyata K, Nakanishi M, Oba M, Ishii T, et al. siRNA-grafted polymer for polyion complex (PIC)-based siRNA delivery: enhancement of PIC stability and gene silencing efficiency. *Biomaterials* 2010;31:8097–105.
- [23] Itaka K, Ishii T, Hasegawa Y, Kataoka K. Biodegradable polyamino acid-based polycations as safe and effective gene carrier minimizing cumulative toxicity. *Biomaterials* 2010;31:3707–14.
- [24] Uchida H, Miyata K, Oba M, Ishii T, Suma T, Itaka K, et al. Odd-even effect of repeating aminoethylene units in the side chain of *N*-substituted polyaspartamides on gene transfection profiles. *J Am Chem Soc* 2011;133:15524–32.
- [25] Harada A, Kataoka K. Formation of polyion complex micelles in an aqueous milieu from a pair of oppositely-charged block copolymers with poly(ethylene glycol) segments. *Macromolecules* 1995;28:5294–9.
- [26] Uchida S, Itaka K, Chen Q, Osada K, Miyata K, Ishii T, et al. Combination of chondroitin sulfate and polyplex micelles of poly(ethylene glycol)-poly{N'-[N-(2-aminoethyl)-2-aminoethyl]aspartamide} block copolymer for prolonged in vivo gene transfection with reduced toxicity. *J Control Release* 2011;155:296–302.
- [27] Nakanishi M, Park J-S, Jang W-D, Oba M, Kataoka K. Study of the quantitative aminolysis reaction of poly( $\beta$ -benzyl L-aspartate) (PBLA) as a platform polymer for functionality materials. *React Funct Polym* 2007;67:1361–72.
- [28] Buyens K, Meyer M, Wagner E, Demeester J, De Smedt SC, Sanders NN. Monitoring the disassembly of siRNA polyplexes in serum is crucial for predicting their biological efficacy. *J Control Release* 2010;141:38–41.
- [29] Mislick KA, Baldeschwieler JD. Evidence for the role of proteoglycans in cation-mediated gene transfer. *Proc Natl Acad Sci USA* 1996;93:12349–54.
- [30] Khalil IA, Kogure K, Akita H, Harashima H. Uptake pathways and subsequent intracellular trafficking in nonviral gene delivery. *Pharmacol Rev* 2006;58:32–45.

# Effect of Polymer Structure on Micelles Formed between siRNA and Cationic Block Copolymer Comprising Thiols and Amidines

R. James Christie,<sup>†</sup> Kanjiro Miyata,<sup>‡,§,||</sup> Yu Matsumoto,<sup>‡,⊥,#</sup> Takahiro Nomoto,<sup>||</sup> Daniel Menasco,<sup>○</sup> Tzai Chung Lai,<sup>○</sup> Matthew Pennisi,<sup>†</sup> Kensuke Osada,<sup>‡,§</sup> Shigeto Fukushima,<sup>†</sup> Nobuhiro Nishiyama,<sup>‡</sup> Yuichi Yamasaki,<sup>‡,§</sup> and Kazunori Kataoka<sup>\*,†,‡,§,||</sup>

<sup>†</sup>Department of Materials Engineering, Graduate School of Engineering, The University of Tokyo, Japan

<sup>‡</sup>Division of Clinical Biotechnology, Center for Disease Biology and Integrative Medicine, Graduate School of Medicine, The University of Tokyo, Japan

<sup>§</sup>Center for NanoBio Integration, The University of Tokyo, Japan

<sup>||</sup>Department of Bioengineering, Graduate School of Engineering, The University of Tokyo, Japan

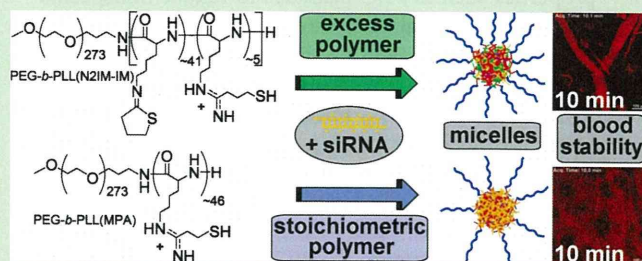
<sup>⊥</sup>Department of Otorhinolaryngology and Head and Neck Surgery, Graduate School of Medicine and Faculty of Medicine, The University of Tokyo, Japan

<sup>#</sup>Department of Otorhinolaryngology and Head and Neck Surgery, Mitsui Memorial Hospital, Japan

<sup>○</sup>Center for Medical Systems Innovation Summer Internship Program, The University of Tokyo, Japan

**S** Supporting Information

**ABSTRACT:** Small interfering RNA (siRNA) has great therapeutic potential for the suppression of proteins associated with disease, but delivery methods are needed for improved efficacy. Here, we investigated the properties of micellar siRNA delivery vehicles prepared with poly(ethylene glycol)-*block*-poly(L-lysine) (PEG-*b*-PLL) comprising lysine amines modified to contain amidine and thiol functionality. Lysine modification was achieved using 2-iminothiolane (2-IT) [yielding PEG-*b*-PLL(N2IM-IM)] or dimethyl 3,3'-dithiobispropionimide (DTBP) [yielding PEG-*b*-PLL(MPA)], with modifications aimed to impart disulfide cross-linking ability without compromising cationic charge. These two lysine modification reagents resulted in vastly different chemistry contained in the reacted block copolymer, which affected micelle formation behavior and stability along with *in vitro* and *in vivo* performance. Amidines formed with 2-IT were unstable and rearranged into a noncharged ring structure lacking free thiol functionality, whereas amidines generated with DTBP were stable. Micelles formed with siRNA and PEG-*b*-PLL(N2IM-IM) at higher molar ratios of polymer/siRNA, while PEG-*b*-PLL(MPA) produced micelles only near stoichiometric molar ratios. *In vitro* gene silencing was highest for PEG-*b*-PLL(MPA)/siRNA micelles, which were also more sensitive to disruption under disulfide-reducing conditions. Blood circulation was most improved for PEG-*b*-PLL(N2IM-IM)/siRNA micelles, with a circulation half-life 3 × longer than naked siRNA. Both micelle formulations are promising for siRNA delivery applications *in vitro* and *in vivo*.



## INTRODUCTION

Small interfering ribonucleic acid (siRNA) is capable of sequence-specific gene silencing without altering the host genome, a property that could be exploited to suppress proteins associated with disease. Thus, there is a strong impetus for development of practical, safe, and effective siRNA-based therapies. However, the inherent properties of siRNA molecules such as large size, anionic nature, and susceptibility to degradation preclude direct use for treatment of disease. Many clever materials have been developed that encapsulate siRNA until the intracellular site of activity is reached to improve its therapeutic activity. Structures formed after encapsulation of siRNA are often referred to as “siRNA carriers” or “siRNA

delivery systems”. To date, the types of materials explored as siRNA carriers include cationic lipids, cyclodextrins, branched and linear polycations, cationic block copolymers, and various peptides. General siRNA delivery strategies and considerations for the design of appropriate carriers have recently been reviewed.<sup>1,2</sup>

Polyion complexes (PICs) are often used to bind and encapsulate siRNA by exploiting its anionic nature.<sup>3</sup> PIC formation is a widely used strategy for preparation of advanced materials

**Received:** May 17, 2011

**Revised:** July 2, 2011

**Published:** August 24, 2011

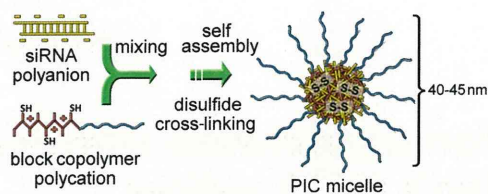


**Figure 1.** Preparation of disulfide cross-linked PIC micelles containing siRNA.

and diagnostics in the field of biomedical technology. PIC-based materials form by electrostatic attraction of oppositely charged polymers, with the release of water solvating charged functional groups providing further energetic gain. These functional materials may exploit single pairs of polyelectrolytes or multiple layering of charged polymers, with polyions from both natural and synthetic origin commonly used. The general strategy of PIC formation has been applied to prepare drug delivery systems, capture analytes for sensors, and form surface coatings, in addition to the formation of polyplexes with nucleic acids as described here.<sup>4–7</sup> PIC formation between nucleic acids and polycations generally results in nanosized structures with morphologies ranging from spheres to rods.<sup>8</sup> Furthermore, advanced PIC-based nucleic acid carriers have been engineered to contain “smart” properties such as PEG palisades to reduce nonspecific interactions with biological components, targeting ligands for tissue-specific accumulation, and also mechanisms for site-specific cargo release through environment-sensitive chemistries.<sup>9–13</sup>

Recently, we reported a PIC micelle siRNA delivery system prepared from the block copolymer poly(ethylene glycol)-*block*-poly(L-lysine) (PEG-*b*-PLL) modified with the cross-linking reagent 2-iminothiolane (2-IT, Traut’s reagent).<sup>14</sup> The resulting block copolymer, termed PEG-*b*-PLL(IM), was designed to contain cationic amidine groups for PIC formation with anionic siRNAs and also free thiols to allow disulfide cross-linking in the micelle core for improved stability. Covalent disulfide cross-links are particularly attractive for micelle core stabilization because they are reversible and more susceptible to cleavage (reduction) at the subcellular site of activity where the levels of natural disulfide reducing agents are higher than in the bloodstream.<sup>15</sup> Disulfide cross-linked PIC micelle formation between siRNA and thiol-modified cationic block copolymer is shown in Figure 1.

Modification of PEG-*b*-PLL with 2-IT improved the quality of the resulting micelles (controlled size and PDI), increased micelle stability, and enhanced siRNA activity in vitro. However, micelles formed only at specific molar ratios of polymer/siRNA, and this optimal ratio increased with increased IM content in the PLL block. One possible explanation for this observed complexation behavior between PEG-*b*-PLL(IM) and siRNA could be related to the instability of amidines formed with 2-iminothiolane. Rearrangement of 2-IT modified amines is known to occur following reaction with amino acids and involves intramolecular reaction of sulfur with the amidine carbon, subsequent release of ammonia, and formation of a *N*-substituted 2-iminothiolane ring. This five-membered ring structure contains an imine bond ( $pK_a \sim 6.7$ ) not an amidine ( $pK_a \sim 12$ ), thus, reducing the positive charge of the block copolymer at pH 7.4.<sup>16,17</sup>

The focus of this work was to better understand the micelle formation behavior between PEG-*b*-PLL(IM) and siRNA, with the hypothesis that formation of *N*-substituted 2-iminothiolanes

affects the formation and properties of micelles. This was accomplished by comparing 2-IT with the analogous amine-reactive amidination reagent, dimethyl 3,3'-dithiobispropionimide (DTBP), to yield PEG-*b*-PLL(MPA). DTBP differs from 2-IT by a methylene unit between the thiol and amidine functional group, which prevents formation of *N*-substituted 2-iminothiolane ring structures due to the instability of a 4-membered ring. Comparison between the two polymer analogues clarified the siRNA complexation behavior previously observed for PEG-*b*-PLL(IM) and also provided insight into the structure–function relationship between the block copolymer component and the properties of resulting micelle structures. Micelle formulations prepared from both block copolymers represent improvements compared to naked siRNA and noncross-linked PICs, and are promising candidates for further development.

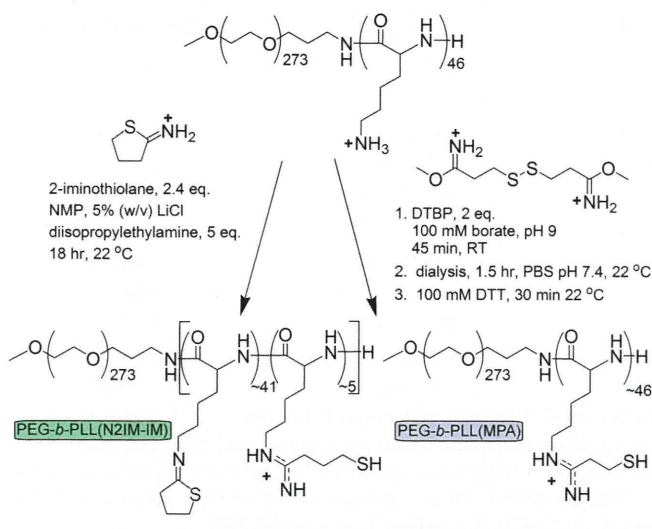
In this study we directly observed both *N*-substituted 2-iminothiolane rings and also linear 1-(4-mercaptobutyl) amidine groups upon <sup>1</sup>H NMR analysis of the reaction product of PEG-*b*-PLL with 2-IT, and have named the polymer “PEG-*b*-PLL(N2IM-IM)”.

## EXPERIMENTAL SECTION

**General.** *N*-Methyl-2-pyrrolidinone (NMP, 99.5% anhydrous), LiCl (>99%), sodium tetraborate decahydrate (99.5%), diisopropylethylamine (DIPEA, 99.5%), 2N HCl solution, D<sub>2</sub>O (99.9%), tetramethylsilane (TMS, 99.5%), and DCl (35% in D<sub>2</sub>O) were obtained from Sigma Aldrich (St. Louis, MO) and used without further purification. 2-Iminothiolane hydrochloride (2-IT), diethyl ether (99+%), dithiothreitol (DTT, molecular biology grade DNase and RNase free), ethylenediamine tetraacetic acid disodium salt dihydrate (EDTA, 99.5%), sodium bicarbonate (99.5–100.3%), sodium dihydrogen phosphate·2H<sub>2</sub>O (99–102%), disodium hydrogen phosphate·12H<sub>2</sub>O (99+%), glutathione (reduced form), and sodium chloride (99+%) were supplied by Wako Pure Chemical Industries (Osaka, Japan). Dimethyl 3,3'-dithiobispropionimide·2HCl (DTBP), Ellman’s reagent [5,5-dithio-bis-(2-nitrobenzoic acid)], 2,4,6-trinitrobenzene sulfonic acid (5% w/v in methanol), and slide-a-lyzer dialysis cassettes (MWCO = 3.5 kDa) were obtained from Thermo Scientific (Rockford IL). Sterile HEPES (1 M, pH 7.3) was purchased from Amresco (Solon, OH). Spectra/Por dialysis tubing (10 kDa MWCO) was acquired from Spectrum Laboratories (Rancho Dominguez, CA). Firefly GL3 luciferase siRNA (sense: 5'-CUU ACG CUG AGU ACU UCG AdTdT-3'; antisense: 5'-UCG AAG UAC UCA GCG UAA GdTdT-3') Cy3-labeled firefly luciferase siRNA, Cy5-labeled firefly luciferase siRNA, and scramble siRNA (sense: 5'-UUC UCC GAA CGU GUC ACG UdTdT-3'; antisense: 5'-ACG UGA CAG GUU CGG AGA AdTdT-3') were synthesized by Hokkaido System Science Co., Ltd. (Hokkaido, Japan) with dye labels attached to the sense strands.

<sup>1</sup>H NMR analysis of PEG-*b*-PLL(N2IM-IM) was conducted in D<sub>2</sub>O containing 0.05% v/v tetramethylsilane and 3 μL/mL DCl solution (35% DCl in D<sub>2</sub>O) at 22 °C using a 300 MHz spectrometer (EX 300, JEOL, Tokyo, Japan). <sup>1</sup>H NMR analysis of PEG-*b*-PLL(MPA) and PEG-*b*-PLL was conducted in the same fashion as PEG-*b*-PLL(N2IM-IM) except without DCl.

Static and dynamic light scattering measurements were performed at 25 °C on a ZetaSizer Nano ZS instrument (Malvern Instruments Ltd., Malvern, U.K.) equipped with a He–Ne laser ( $\lambda = 633$  nm) as the incident beam with samples (16 μL) loaded into a Zen 2112 low-volume cuvette. Absorbance and fluorescence measurements were performed with NanoDrop ND-1000 and ND-3300 instruments (NanoDrop Technologies Inc., Rockland DE), respectively.

Scheme 1. Synthesis of PEG-*b*-PLL Derivatives

The luciferase-expressing mouse melanoma cancer cell line, B16F10-luc, was purchased from Caliper LifeScience (Hopkinton, MA). Dulbecco's modified eagle's medium (DMEM) was obtained from Sigma Aldrich (St. Louis, MO). Fetal bovine serum was provided by Dainippon Sumitomo Pharma Co. (Osaka, Japan). Falcon Easy-Grip 35 × 10 mm vacuum gas plasma-treated polystyrene tissue culture dishes were obtained from BD Biosciences (San Jose, CA). Luciferin was purchased from Summit Pharmaceutical International (Tokyo, Japan). Luciferase bioluminescence in B16F10-luc cells was measured using an ATTO Kronos Dio photon countable incubator (ATTO Corp., Tokyo, Japan).

**Synthesis of PEG-*b*-PLL(N2IM-IM).** PEG-*b*-PLL copolymer was synthesized as previously described, comprising a 12000 MW PEG segment and a 45 amino acid PLL segment.<sup>13,18</sup> Iminothiolane modification of PEG-*b*-PLL was achieved by reacting primary amino groups contained in the side chains of PLL with 2-IT, as outlined in Scheme 1. First, 50 mg PEG-*b*-PLL (0.12 mmol amine, 1 equiv) was added to 2 mL NMP containing 5 wt % LiCl and the reaction vessel was purged with Ar and then capped with a septum. The polymer solution was placed into an oil bath at 50 °C and stirred for 30 min to completely dissolve all solids. After dissolution of polymer, the solution was removed from heat and cooled to 22 °C. Next, DIPEA (100 μL, 1.1 mmol, 5 equiv relative to Lys amines) was added to the polymer solution under Ar through the septum. Finally, 2-iminothiolane·HCl (39 mg, 0.28 mmol, 2.4 equiv relative to lysine amines) was added directly to the polymer solution. The reaction continued with stirring for 18 h at 22 °C under an argon atmosphere. After 18 h, the reaction was terminated by precipitation into a 10× volume excess of dry diethyl ether. Precipitated product was washed several times with ether and dried under vacuum to a constant mass. Crude product was redissolved in PBS buffer (10 mM phosphate, 150 mM NaCl, pH 6.0) and then dialyzed (SpectraPor7, 10 kDa MWCO) against PBS pH 6.0 for one day and distilled water for one day with frequent media changes. Dialyzed polymer solution was passed through a 0.2 μm filter and then lyophilized. Yield: 55 mg (96%), white powder. The degree of lysine modification was determined from the <sup>1</sup>H NMR spectra recorded in acidic D<sub>2</sub>O (Figure 2) by the peak intensity ratio of the β, γ, and δ-methylene protons of Lys ((CH<sub>2</sub>)<sub>3</sub>, δ = 1.3–1.9 ppm) to the sum of peak intensities of methylene protons from the C4 carbon of N-substituted 2-iminothiolane groups and the protons of trimethylene units of mercaptopropyl groups (HS-(CH<sub>2</sub>)<sub>3</sub>, δ = 2.1, 2.6, and 2.8 ppm). The calculated IM introduction rate was 95%. The ratio of 1-(4-mercaptobutyl) amidine groups to N-substituted 2-iminothiolane

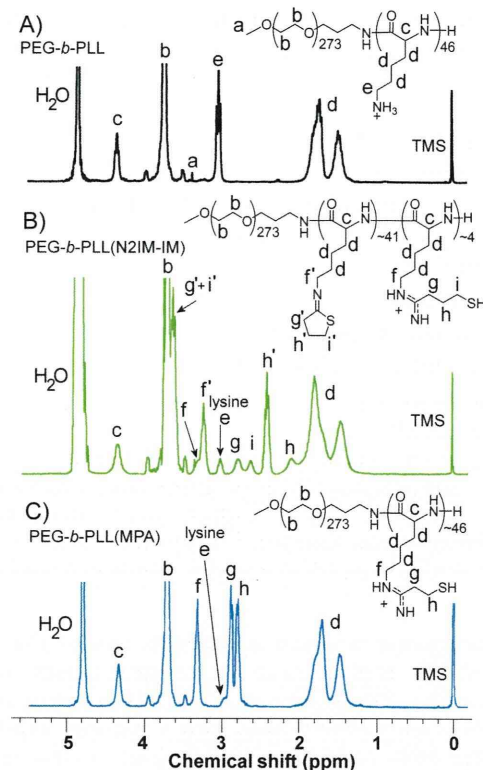


**Figure 2.** <sup>1</sup>H NMR spectra of PEG-*b*-PLL and modification products. Spectra were recorded at 300 MHz, 25 °C in D<sub>2</sub>O (A,C) or D<sub>2</sub>O containing 3 μL/mL 35% DCl solution (B). Residual lysine residues are not included in the chemical structures shown in (B) and (C).

groups was determined by the peak intensity ratios of methylene protons from the C4 position on N-substituted 2-iminothiolane groups (2.4 ppm) and protons of trimethylene units of mercaptopropyl groups (HS-(CH<sub>2</sub>)<sub>3</sub>, δ = 2.1, 2.6, and 2.8 ppm). The ratio of 1-(4-mercaptobutyl) amidine to N-substituted 2-iminothiolane was ~0.25.

**Synthesis of PEG-*b*-PLL(MPA).** PEG-*b*-PLL(MPA) was synthesized by reaction of lysine primary amines with amido esters contained in DTBP as shown in Scheme 1. First, PEG-*b*-PLL (300 mg, 0.7 mmol amines, 1 equiv) of the same parent stock used for synthesis of PEG-*b*-PLL(N2IM-IM) was dissolved in 100 mM sodium borate, pH 9.0 (60 mL) and then DTBP·HCl (439 mg, 1.4 mmol, 2 equiv relative to lysine amines) was added to the polymer solution. The reaction was stirred at room temperature for 45 min and then transferred to slide-a-lyzer dialysis cassettes (MWCO 3500) and dialyzed against PBS (10 mM phosphate, 150 mM NaCl, pH 7.4) for 1.5 h to remove unreacted DTBP. The reaction mixture was recovered and then DTT (300 mg) was added to generate the free sulfhydryl in polymer-reacted DTBP. The reaction was stirred at room temperature for 30 min and then transferred to slide-a-lyzer dialysis cassettes (MWCO 3500). Dialysis was performed against 10 mM PBS, pH 6.0 for 2 h and then distilled water for 2 h with rapid stirring and frequent exchange of dialysis media. The purified polymer solution was passed through a 0.2 μm filter and lyophilized. Yield: 299 mg (73%), white powder. The degree of DTBP introduction was determined from the <sup>1</sup>H NMR spectra shown in Figure 2 by the peak intensity ratio of the β, γ, and δ-methylene protons of Lys ((CH<sub>2</sub>)<sub>3</sub>, δ = 1.3–1.9 ppm) to the protons of mercaptoethyl groups (HS-(CH<sub>2</sub>)<sub>2</sub>, δ = 2.7–2.9 ppm). The calculated degree of lysine modification was 95%.

**Analysis of Thiol Content in Block Copolymers.** Free thiol content in modified block copolymers was determined by Ellman's assay.<sup>19</sup> Polymer solutions (5 mg/mL) were incubated in 10 mM HEPES buffer containing 5 mM EDTA and 15 mM DTT for 30 min

Table 1. Summary of Polymer and Micelle Properties

	PEG- <i>b</i> -PLL <sup>l</sup>	PEG- <i>b</i> -PLL(N2IM-IM)	PEG- <i>b</i> -PLL(MPA)
MW <sup>a</sup>	19600	22000	23350
% modified lysines <sup>b</sup>	0	95	95
% thiol content <sup>c</sup>	0.7 ± 0.04	11 ± 2.5	90 ± 12
polymer/siRNA molar ratio with maximum SLI at pH 7.4/5.0 <sup>d</sup>	1.2/ND	≥7.6/1.4	1.2/1.3
micelle size (d.nm) <sup>e,f,g</sup>	194 ± 15	42.4 ± 2.2	41.8 ± 2.1
micelle PDI <sup>e,g</sup>	0.44 ± 0.1	0.07 ± 0.02	0.05 ± 0.02
micelle ζ potential <sup>g</sup>	ND	−1.99 ± 0.47	−0.50 ± 1.26
micelle stability in 600 mM NaCl <sup>d,g,h</sup>	<5%	86%	43%
% remaining thiol in cross-linked micelles <sup>e,i</sup>	ND	52 ± 0.54	3.7 ± 0.27
maximum gene silencing <sup>e,j</sup>	<5%	~12%	~40%
circulation half-life <sup>e,k</sup>	~3 min	~10 min	~6 min

<sup>a</sup>Including chloride counterion. <sup>b</sup>Determined by <sup>1</sup>H NMR. <sup>c</sup>Determined by Ellman's Assay. <sup>d</sup>Determined by static light scattering, 25 °C. <sup>e</sup>Determined by dynamic light scattering, pH 7.4, 25 °C. <sup>f</sup>Reported as the z-average cumulant mean diameter. <sup>g</sup>Cross-linked micelles prepared at the polymer/siRNA molar ratio of max SLI. <sup>h</sup>Stability relative to cross-linked micelles in 10 mM HEPES, pH 7.4. <sup>i</sup>Expressed relative to the free thiol content measured in polymer before micelle formation. <sup>j</sup>Determined in B16F10-luc cancer cells, 200 nM siRNA, 48 h. <sup>k</sup>Determined by in vivo confocal intravitral microvideography, 24 μg siRNA injection. <sup>l</sup>Structures formed with siRNA may not be micelles due to their large size and PDI.

at room temperature to reduce any disulfides present. The reduced polymer solution was placed on ice and handled in a timely manner at 0–4 °C until the addition of Ellman's reagent. After reduction, DTT was removed from the polymer solution using a NanoSep centrifugation device (3000 MWCO). Samples were subjected to three successive concentration/rinsing cycles with 10 mM HEPES containing 5 mM EDTA as the rinsing buffer. After the final centrifugation cycle, concentrated polymer solution was collected and diluted to its original volume. The final flow-through fraction was also collected and diluted in the same manner as the polymer-containing fraction to determine the amount of DTT remaining in the sample. Polymer and flow through samples were subjected to Ellman's assay according to the manufacturers protocol and sample absorbance was measured at 412 nm. Free thiol content of solutions was determined from a standard curve generated with reduced glutathione, and the thiol content in the polymer fraction was obtained by subtracting the thiol content in the flow-through fraction to correct for residual DTT. PEG-*b*-PLL was analyzed as a negative control in a similar fashion, except the polymer solution (5 mg/mL) was used directly without DTT incubation.

**Complexation of Block Copolymers with siRNA.** Block copolymer complexation and micelle formation with siRNA was studied as a function of the molar ratio of polymer/siRNA using the polymer molecular weights shown in Table 1. It should be noted that siRNA contains 40 negative charges and the poly(L-lysine) segment in the block copolymer contains ~46 units. Thus, if all modified PLL side-chains are charged the polymer/siRNA molar ratio and +/- charge ratio are nearly interchangeable. Polymer samples were dissolved in 10 mM HEPES buffer (pH 7.4) at a concentration of 5 mg/mL and aliquots were further diluted from this stock solution for preparation of complexation mixtures with siRNA. PEG-*b*-PLL(MPA) polymer solutions were diluted first with HEPES buffer to generate a solution twice the concentration desired for mixing with siRNA, and then 1:1 with HEPES buffer containing 30.54 mg/mL DTT. PEG-*b*-PLL(N2IM-IM) polymer solutions were reduced by direct addition of DTT to the 5 mg/mL polymer stock solution to yield 15.25 mg/mL DTT. Polymer solutions were incubated for 30 min at room temperature after addition of DTT to ensure cleavage of any disulfides present. Complexation was achieved by mixing polymer solution with siRNA (15 μM in 10 mM HEPES buffer, pH 7.4) at a volume ratio of 1:2 (polymer/siRNA) and PIC micelles were allowed to form for 24 h at 25 °C. For micelle formation at pH 5.0, both reduced polymer and siRNA solutions were acidified with appropriate volumes of 0.05 M HCl prior to mixing, then combined

immediately. Disulfide cross-linked micelles were prepared by dialysis (slide-a-lyzer cassette (MWCO 3.5 kDa)) against 10 mM HEPES pH 7.4 containing 0.5% v/v DMSO for 2 days, followed by 2 days of dialysis against HEPES for removal of DMSO. DMSO was included in the dialysis buffer to assist in disulfide formation, as it is a mild oxidant specific toward thiols.<sup>20</sup> All disulfide cross-linked micelle samples were prepared at the polymer/siRNA molar ratio that exhibited maximum light scattering intensity in optimization experiments, polymer/siRNA = 7.6 for PEG-*b*-PLL(N2IM-IM) and 1.3 for PEG-*b*-PLL(MPA). Free thiol content in cross-linked micelles was determined using the Elman's assay according to the manufacturers protocol by sample absorbance at 412 nm and a standard curve generated with reduced glutathione. PEG-*b*-PLL(N2IM-IM) micelles were used directly for the assay whereas PEG-*b*-PLL(MPA)/siRNA micelles were concentrated 4-fold using NanoSep centrifugation devices (3000 MWCO) to yield a micelle solution with a theoretical thiol content within the range of the calibration curve.

**Characterization of Micelles.** PIC micelle solutions were analyzed by static and dynamic light scattering (DLS) to determine scattered light intensity (SLI) and PIC micelle size/PDI, respectively. Size distributions were determined by cumulant and histogram analysis of DLS data. Results are shown as the z-average diameter (cumulant mean) with the polydispersity index (PDI) (defined in the ISO standard document 13321:1996) and histogram of size distribution, as determined by the software provided by the manufacturer. The ζ-potentials of cross-linked PIC micelles prepared at the polymer/siRNA molar ratio with maximum SLI were measured in 10 mM HEPES buffer (pH 7.4) containing 150 mM NaCl at 37 °C. All samples were equilibrated to the defined temperature for 2 h prior to measurement. For fluorescence quenching experiments, PIC micelle solutions were prepared at various polymer/siRNA molar ratios as described above except Cy3-labeled GL3 siRNA was used. After 24 h incubation in the dark at 25 °C, the fluorescence intensity was measured with a NanoDrop ND-3300 instrument using white LED excitation.

**In Vitro Stability of Micelles.** Disulfide cross-linked PIC micelle stability was measured as a function of NaCl concentration in the presence or absence of the disulfide reducing agent DTT. Cross-linked micelle samples were diluted 1:1 with NaCl solution at desired concentrations and incubated at 37 °C for 24 h. Samples subjected to disulfide reducing conditions were diluted in the same fashion as above, however, with NaCl solutions containing 200 mM DTT. After the 24 h incubation period, samples were measured by static and dynamic light scattering, as described in the micelle characterization section.

**TEM Analysis of Cross-Linked Micelles.** Cross-linked micelle morphology was directly observed by transmission electron microscopy (TEM). For each analysis, the nucleic acid stain uranyl acetate (10  $\mu\text{L}$  of a 2% w/v solution) was deposited onto a glass slide followed by sample solution (10  $\mu\text{L}$ ). This mixture was allowed to stand for 30 s in order to achieve effective staining. A carbon-coated 400 mesh Cu grid (Nisshin EM) was then immersed into the sample, allowing both sides of the grid to become fairly saturated. The grid was air-dried on a piece of filter paper and then transferred to a H-7000 TEM (Hitachi Ltd., Tokyo, Japan) for imaging. Images were recorded at optical magnifications of 50000 and 80000 with an acceleration voltage of 75 kV.

Micelle size distributions were determined from TEM images using ImageJ (available online at <http://rsb.info.nih.gov/ij/download.html>). TEM images previously modified by the addition of a scale bar were uploaded onto a computer and opened with ImageJ. A pixel to nanometer conversion value was generated by manually drawing a line on the scale bar and utilizing the program's built in Analyze  $\rightarrow$  Set Scale command. Following creation of the pixel:nanometer conversion factor, lines were drawn by hand on each individual particle and their nanometer value was obtained via the Analyze  $\rightarrow$  Measure command. A total of 46 particles were analyzed from each image. The raw data was imported into Microsoft Excel and histograms were generated.

**In Vitro Gene Silencing.** The gene silencing activity of siRNA incorporated in cross-linked micelles was determined in B16F10 murine melanoma cancer cells stably expressing luciferase (B16F10-luc), with luciferase targeted for gene knockdown. Cross-linked micelles containing GL3 (target) or scramble (off-target) siRNA were prepared as described above. Cells were cultured in Dulbecco's modified eagle's medium (DMEM) containing 10% fetal bovine serum (FBS). B16F10-luc cells were seeded onto 35 mm Petri dishes (25000 cells/dish) and allowed to attach for 24 h. After cell attachment, the media was removed and replaced with media (2 mL) containing 100  $\mu\text{M}$  luciferin and cross-linked micelles corresponding to 200 nM micelle-encapsulated siRNA. For each analysis, control cell samples were prepared by addition of media diluted with HEPES instead of micelle solution. The total dilution of media after addition of luciferin and micelle solution was less than 200  $\mu\text{L}$  additives per 10 mL of media. Samples were placed into a Kronos real-time photon-countable incubator and the luminescence intensity was measured periodically over a 55 h time period, with the temperature and  $\text{CO}_2$  maintained at 37  $^\circ\text{C}$  and 5%. The amount of gene silencing was determined by dividing the average luminescence intensity of treated samples by the average luminescence intensity of control samples,  $n = 4$ .

**In Vivo Micelle Stability.** SiRNA incorporating micelle stability in the blood compartment was evaluated using intravital confocal videography in live mice. All picture/movie acquisitions were performed using a Nikon A1R confocal laser scanning microscope system attached to an upright ECLIPSE FN1 (Nikon Corp., Tokyo, Japan) equipped with a 20 $\times$  objective, 640 nm diode laser, and a band-pass emission filter of 700/75 nm. The pinhole diameter was set to result in a 10  $\mu\text{m}$  optical slice. Eight-week-old female BALB/c nude mice (Oriental Yeast Co., Ltd., Tokyo, Japan) were anesthetized with 2.0–3.0% isoflurane (Abbott Japan Co., Ltd., Tokyo, Japan) using a Univentor 400 Anaesthesia Unit (Univentor Ltd., Zejtun, Malta). Mice were then subjected to lateral tail vein catheterization with a 30-gauge needle (Becton, Dickinson and Co, Franklin Lakes, NJ, U.S.A.) connected to a nontoxic medical grade polyethylene tube (Natsume Seisakusho Co., Ltd., Tokyo, Japan). Anesthetized mice were placed onto a temperature-controlled pad (Thermoplate; Tokai Hit Co., Ltd., Shizuoka, Japan) integrated into the microscope stage and maintained in a sedated state throughout the measurement. Ear lobe dermis was observed without surgery and was easily fixed beneath a coverslip with a single drop of immersion oil. Data was acquired in video mode for 3 min (30 frames/sec), followed by snapshots every 1 min thereafter. All animal experimental procedures

were performed in accordance with the Guide for the Care and Use of Laboratory Animals as stated by the National Institutes of Health.

Micelles prepared with Cy5-labeled siRNA at the polymer/siRNA molar ratio corresponding to maximum SLI (7.6 for PEG-*b*-PLL(N2IM-IM) and 1.2 for PEG-*b*-PLL(MPA)) were injected (200  $\mu\text{L}$  of 9.2  $\mu\text{M}$  siRNA,  $\sim 24 \mu\text{g}$  total siRNA) via the tail vein 10 s after the start of video capture. Micelles prepared with PEG-*b*-PLL(N2IM-IM) or PEG-*b*-PLL(MPA) and siRNA were cross-linked, as described above before injection.

Video data was analyzed by selecting regions of interest (ROIs) within blood vessels or extravascular skin tissue and the average fluorescence intensity per pixel for each time point was determined using the Nikon NIS-Elements C software provided by the manufacturer. To produce the blood retention profiles shown in Figure 6, vein fluorescence data was expressed relative to the maximum observed value. First, the background fluorescence intensity was determined from video captured during the 10 s before sample injection. This background value was then subtracted from the average pixel intensities measured after micelle injection to create background-corrected intensities for each time point. Next, relative fluorescence intensities were determined by dividing the average fluorescence intensity at each time point by the maximum observed fluorescence intensity (typically observed  $\sim 1$  min). Analysis of tissue fluorescence intensity was performed in the same manner, without normalizing to the maximum observed value. Each experiment was performed in duplicate in separate animals, with representative data from a single animal shown in Figure 6. Individual circulation data for each mouse is provided as Supporting Information. A detailed description of the microscope apparatus and mouse positioning for intravital confocal micro videography, as well as examples of data workup showing ROIs can be found in our previously published report.<sup>21</sup>

## RESULTS

**Modification of PEG-*b*-PLL with 2-IT.** PEG-*b*-PLL was reacted with excess 2-IT under organic conditions, as previously described, except 2-IT was added directly to the reaction mixture as a solid instead of dropwise addition of a solution.<sup>14</sup> The reaction proceeded by nucleophilic attack of lysine amine groups on the imine carbon contained in 2-IT, followed by ring-opening and generation of the free sulfhydryl (which may subsequently react with the amidine carbon as discussed below). Analysis of the PEG-*b*-PLL(N2IM-IM) polymer product by  $^1\text{H}$  NMR spectroscopy showed that the desired modification was successful, as the lysine  $\epsilon\text{-CH}_2$  peak was shifted downfield and methylene peaks corresponding to N2IM and IM groups appeared in the spectrum (Figure 2). Both linear 1-(4-mercaptobutyl) amidine and cyclic N-substituted 2-iminothiolane groups were observed in the product, with the majority of side chains ( $\sim 75\%$ ) being in the closed ring form based on integration values. Nearly complete conversion (95%) of lysine amine groups was achieved by this synthesis procedure. It should be noted that 2 mol equiv of 2-IT (relative to lysine amines) is necessary to achieve nearly complete modification of lysine amines. Addition of 1 mol equiv of 2-IT resulted in only  $\sim 60\%$  conversion of lysine amines (data not shown).

2-IT modified polymer product was soluble in buffer despite the loss of charged functional groups. However, polymer self-association at 10 mg/mL interfered with  $^1\text{H}$  NMR analysis in  $\text{D}_2\text{O}$  and acidification of the sample greatly clarified the spectrum. PEG-*b*-PLL(N2IM-IM) polymer solution showed very little light scattering at the concentration used for siRNA complexation (1.67 mg/mL) and addition of siRNA to the polymer

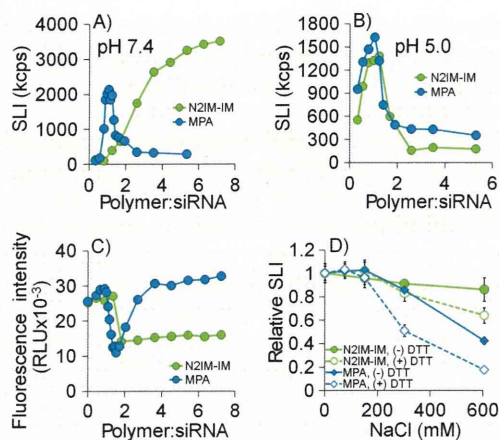


**Figure 3.** Light scattering behavior of siRNA and PEG-*b*-PLL(*X*) (*X* = N2IM-IM or MPA) mixtures, fluorescence quenching, and the stability of resulting cross-linked micelles. (A) Complexation of block copolymers with siRNA at pH 7.4, 25 °C. (B) Complexation of block copolymers with siRNA at pH 5.0, 25 °C. (C) Fluorescence quenching of Cy3-siRNA/block copolymer mixtures at pH 7.4, 25 °C. (D) Stability of disulfide cross-linked micelles following 24 h incubation at 37 °C in NaCl solutions with or without disulfide reducing agent (DTT). Data represents the average value  $\pm$  standard deviation,  $n = 3$ . All polymer/siRNA ratios are molar ratios.

solution resulted in a 10-fold increase in scattered light intensity. A detailed analysis of polymer solution light scattering at pH 7.4 and 4.0 is available as Supporting Information.

**Modification of PEG-*b*-PLL with DTBP.** PEG-*b*-PLL was modified with DTBP under aqueous conditions. Nucleophilic reaction of lysine primary amine groups with imidoester groups contained in DTBP resulted in formation of the amidine with concurrent release of methanol. The reaction pH of 9.0 was chosen to minimize side reactions that are described to occur with imidoesters below pH 8.0.<sup>22</sup> A molar excess amount of DTBP was used to minimize polymer cross-linking, which is expected to occur due to the bifunctional nature of this reagent. A total of 2 molar equiv of DTBP relative to lysine amines used in the polymer modification reaction corresponded to 4 equiv of reactive amido esters. Unreacted DTBP was removed from the reaction mixture prior to disulfide cleavage of polymer-reacted DTBP to allow more efficient reduction with DTT. Reaction of the DTBP-modified polymer with DTT resulted in cleavage of the internal disulfide and generation of the desired 1-(3-mercaptopropyl) amidine functionality. DTT was removed quickly and efficiently ( $\sim$ 4 h) using high surface area slide-a-lyzer dialysis cassettes, as DTT was not detected in the <sup>1</sup>H NMR spectrum of the obtained product (Figure 2). Successful modification of lysine amines with DTBP was confirmed by <sup>1</sup>H NMR spectroscopy, as indicated by the downfield shift of lysine  $\epsilon$ -CH<sub>2</sub> groups and the appearance of two methylene peaks corresponding to those found in DTBP (Figure 2). The degree of lysine modification was 95% under the reaction conditions used in this study.

**Analysis of Thiol Content in Modified PEG-*b*-PLLs.** Free thiol content in PEG-*b*-PLL(N2IM-IM) and PEG-*b*-PLL(MPA) was determined using Ellman's assay, which is based on reaction of 5,5-dithio-bis-(2-nitrobenzoic acid) with thiols at basic pH to generate a colored thiolate derivative. The measured thiol content was quite different between PEG-*b*-PLL(N2IM-IM) and PEG-*b*-PLL(MPA), as shown in Table 1. PEG-*b*-PLL(MPA)

thiol content was near the theoretical value assuming complete reaction of lysine amines ( $90 \pm 10\%$ ), whereas PEG-*b*-PLL(N2IM-IM) thiol content was much lower ( $11 \pm 2\%$ ). The low amount of free sulfhydryl detected in PEG-*b*-PLL(N2IM-IM) is consistent with the formation of N-substituted 2-iminothiolanes, which lack free thiol functionality.

**Preparation and Characterization of PIC Micelles Formed with siRNA.** PIC micelles formed spontaneously upon mixing polymer and siRNA solutions under reducing conditions, as evidenced by increased scattered light intensity and the presence of particles less than 100 nm in size with low PDI ( $<0.1$ , i.e., spherical). At pH 7.4, PIC micelles formed at higher polymer/siRNA molar ratios for PEG-*b*-PLL(N2IM-IM) (polymer/siRNA = 3.6–7.6) and only at near stoichiometric ratios for PEG-*b*-PLL(MPA) (polymer/siRNA = 1.0–1.3, Figure 3A). Addition of excess polymer in the case of PEG-*b*-PLL(MPA) resulted in a sharp decrease in SLI, showing that excess polycation disrupts micelle formation. DLS analysis of micelle solutions revealed the formation of narrowly dispersed (PDI  $<0.1$ ) particles 40–45 nm in size at the optimal polymer/siRNA mixing ratio for both block copolymers, which is consistent with values expected for spherical micelle structures (Table 1). Detailed light scattering data for complexation solutions (non-cross-linked) at each polymer/siRNA molar ratio is available as Supporting Information. Analysis of the  $\zeta$ -potential of cross-linked micelle structures formed at the optimal polymer/siRNA molar ratio indicated a near-neutral value for both PEG-*b*-PLL(N2IM-IM) and PEG-*b*-PLL(MPA), which is expected for core–shell micelle structures where the core charge is shielded by the PEG corona (Table 1). Essentially no free-thiol was detected in cross-linked micelles prepared with PEG-*b*-PLL(MPA), but  $\sim$ 50% free thiol (relative to the original 11% thiol-containing PLL side chains measured in polymer only) was observed in micelles prepared with PEG-*b*-PLL(N2IM-IM) when subjected to Ellman's assay (Table 1). This result shows that both free thiol content and disulfide cross-linking efficiency was reduced in PEG-*b*-PLL(N2IM-IM).

Complexation behavior between PEG-*b*-PLL(N2IM-IM) and siRNA changed under acidic conditions, whereas PEG-*b*-PLL(MPA) complexation behavior with siRNA did not (Figure 3B). For PEG-*b*-PLL(N2IM-IM), the polymer/siRNA molar ratios corresponding to the maximum SLI value shifted from  $\sim$ 7.6 to lower values near the stoichiometric region. This observation confirmed that protonation of imines present in N-substituted 2-iminothiolane structures can restore the cationic nature of PEG-*b*-PLL(N2IM-IM). On the other hand, PEG-*b*-PLL(MPA) micelle formation behavior was unaffected by lowering the pH of complexation conditions and the polymer/siRNA molar ratio for maximum SLI remained in the stoichiometric region at both pH 7.4 and 5.0. Micelle size and PDI at the polymer/siRNA molar ratio corresponding to maximum SLI did not change for either polymer upon complexation at lower pH (data not shown).

**Fluorescence Quenching Studies.** PEG-*b*-PLL(N2IM-IM) and PEG-*b*-PLL(MPA) complexation with siRNA was also investigated by monitoring the fluorescence quenching of Cy3-labeled siRNA (Figure 3C). Fluorescence quenching is expected to occur only upon formation of micelle structures through dye–dye interactions or interaction with amines contained in the micelle core.<sup>23–25</sup> Cy3 fluorescence was quenched considerably upon formation of micelles between both block copolymers and siRNA. For PEG-*b*-PLL(MPA), maximum fluorescence quenching was concurrent with the polymer/siRNA molar ratio that resulted in the maximum SLI observed in light scattering

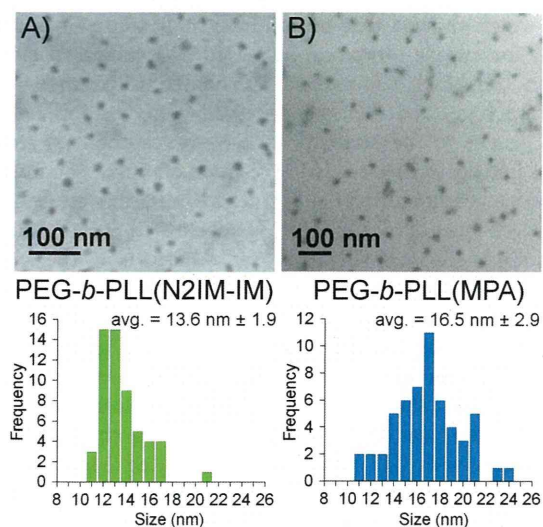


**Figure 4.** TEM images showing the morphology of cross-linked micelles. (A) PEG-*b*-PLL(N2IM-IM)/siRNA micelles, 80K magnification. (B) PEG-*b*-PLL(MPA) micelles, 50K magnification. The resulting size histograms from measuring the uranyl acetate stained micelle cores are shown below each image.

measurements. Addition of excess PEG-*b*-PLL(MPA) to the complexation mixture resulted in complete recovery of fluorescence intensity, indicating that the micelle structure was not maintained at high polymer/siRNA ratios. However, complexation of Cy3 siRNA with PEG-*b*-PLL(N2IM-IM) resulted in fluorescence quenching at polymer/siRNA ratio of  $\sim 1.8$  and quenching was maintained up to the polymer/siRNA ratio of 7.6, indicating that polymer/siRNA complexes were unaffected by excess block copolymer. This result corroborates well with light scattering observations where the SLI of solutions prepared with PEG-*b*-PLL(MPA) and siRNA decreased at polymer:siRNA molar ratios greater than  $\sim 1.4$  (showing micelle dissociation), whereas complexation solutions prepared with PEG-*b*-PLL(N2IM-IM) never exhibited a decrease in SLI up to the polymer/siRNA molar ratio of 7.6 (showing micelle structure is maintained).

**In Vitro Micelle Stability.** Cross-linked micelle stability was determined as a function of NaCl concentration in the presence or absence of the disulfide reducing agent DTT (Figure 3D). Increased NaCl concentration is expected to interfere with the ionic interactions between cationic polymer and siRNA, thus, disrupting micelle structures. This experiment was not intended to mimic biological conditions, but as a reference, the biological NaCl concentration is  $\sim 150$  mM. In general, micelles prepared with siRNA and PEG-*b*-PLL(N2IM-IM) were more stable than those prepared with PEG-*b*-PLL(MPA). In the absence of DTT, micelles prepared with PEG-*b*-PLL(N2IM-IM) remained stable up to 600 mM NaCl, whereas micelles prepared with PEG-*b*-PLL(MPA) showed a significant decrease in SLI at 600 mM NaCl. Addition of DTT to the micelle solution resulted in an  $\sim 20\%$  decrease in SLI at 600 mM NaCl for PEG-*b*-PLL(N2IM-IM), while the SLI of PEG-*b*-PLL(MPA) micelle solutions decreased to a greater extent ( $\sim 30\text{--}50\%$ ) upon disulfide reduction at both 300 and 600 mM NaCl.

**Micelle Morphology.** Direct observation of cross-linked micelles by TEM showed uniform spherical structures less than 50 nm in size (Figure 4). The dark spheres in the TEM images

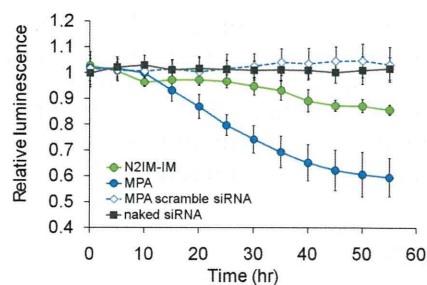


**Figure 5.** In vitro gene knockdown of luciferase in B16F10-luc cells. SiRNA was incorporated within cross-linked micelles prepared with PEG-*b*-PLL(X) (X = N2IM-IM or MPA) and introduced to cells at 200 nM siRNA. Data is presented as the ratio of treated sample luminescence to nontreated controls  $\pm$  the standard deviation,  $n = 4$ .

correspond to the micelle core, as uranyl acetate specifically stains nucleic acids. Micelle core diameters were found to be 13.6 nm for PEG-*b*-PLL(N2IM-IM)/siRNA and 16.5 nm for PEG-*b*-PLL(MPA)/siRNA, both with narrow size distribution.

**In Vitro Gene Silencing.** The ability of micelles to deliver and release antiluciferase siRNA aimed to inhibit luciferase expression was determined in B16F10 murine melanoma cells stably expressing luciferase. In vitro gene silencing was highest when siRNA was administered encapsulated within micelles prepared with PEG-*b*-PLL(MPA), as shown in Figure 5. PEG-*b*-PLL(MPA)/siRNA micelle treated cells showed a modest ( $\sim 40\%$ ) decrease in luminescence between 10 and 55 h, while PEG-*b*-PLL(N2IM-IM)/siRNA micelles showed a smaller ( $\sim 12\%$ ) decrease in luminescence between 25 and 55 h. No cytotoxicity was observed for PEG-*b*-PLL(N2IM-IM)/siRNA or PEG-*b*-PLL(MPA)/siRNA micelles at siRNA concentrations up to 1000 nM, showing that luciferase knockdown was not due to reduced cell metabolism as a result of micelle introduction (see Supporting Information). Negligible luciferase knockdown was observed for naked siRNA or PEG-*b*-PLL(MPA)/siRNA micelles containing scramble siRNA, indicating that encapsulation within a micelle carrier is essential and also that the gene silencing was due to the siRNA effect and not due to the polymer used for micelle formation. No gene silencing was observed for PEG-*b*-PLL/siRNA micelles prepared at polymer/siRNA molar ratio of 1.2 (Table 1).

**In Vivo Micelle Stability.** Micelle behavior in the bloodstream was observed in mouse ear lobe dermis following I.V. injection. Naked siRNA was rapidly removed from the bloodstream (Figure 6A), with a half-life of approximately 3 min. Blood circulation time was improved by incorporating siRNA into disulfide-cross-linked micelle carriers, as the half-life increased to  $\sim 6$  min for micelles prepared with PEG-*b*-PLL(MPA) and  $\sim 10$  min for micelles prepared with PEG-*b*-PLL(N2IM-IM). Cy5 fluorescence intensity remained high for the first  $\sim 2$  min for both disulfide-cross-linked micelle formulations but then rapidly decreased for PEG-*b*-PLL(MPA), with a profile similar to naked siRNA. The difference in blood vessel retention is clearly seen in Figure 6C, where Cy5 fluorescence remained high for PEG-*b*-PLL(N2IM-IM)/siRNA micelles after 10 min. No aggregates were visible in the bloodstream for any of the formulations following injection.

Extravasation of Cy5 into the surrounding skin tissue was apparent for naked siRNA and PEG-*b*-PLL(MPA)/siRNA micelles (Figure 6B). Extravasation is expected to occur only for low molecular weight species and, thus, indicates dissociation of the

micelles and possibly degradation of siRNA. Cy5 fluorescence increased in the tissue region more rapidly for PEG-*b*-PLL(MPA)/siRNA micelles compared to PEG-*b*-PLL(N2IM-IM)/siRNA micelles. Tissue fluorescence for PEG-*b*-PLL(N2IM-IM)/siRNA micelles slowly increased over the 60 min observation period and never peaked (Figure 6B).

## DISCUSSION

The focus of this work was to better understand the mechanism of polyion complex micelle formation between PEG-*b*-PLL(N2IM-IM) and siRNA, and also to observe the effects of polymer structure on micelle properties. Interest regarding the mechanism of micelle formation between PEG-*b*-PLL(N2IM-IM) and siRNA was sparked by observations from our previous

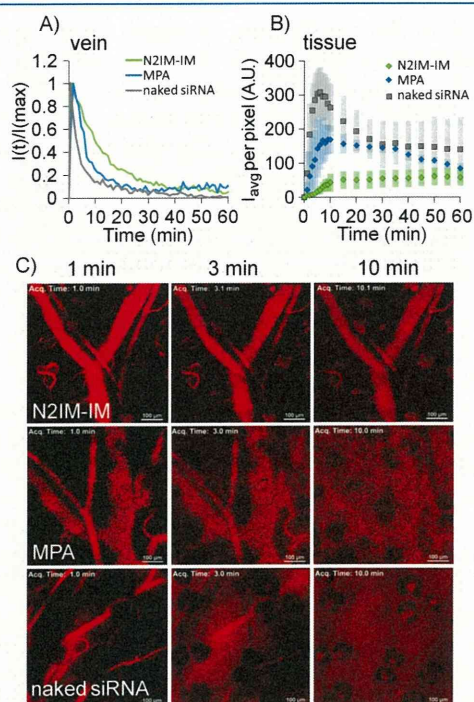


**Figure 6.** Behavior of siRNA incorporating micelles prepared with PEG-*b*-PLL(X) (X = N2IM-IM or MPA) following intravenous injection. (A) Residence time of Cy5 in the bloodstream normalized to the maximum observed intensity. (B) Cy5 fluorescence in the extravascular skin tissue, each data point represents the mean value  $\pm$  the standard deviation of four regions of interest. (C) Snapshots of ear lobe dermis at 1, 3, and 10 min with Cy5 fluorescence shown as red. The scale bar represents 100  $\mu$ m in each image. Representative data from one mouse for each sample is shown in A–C.

work which showed that the optimal molar ratio of polymer/siRNA for micelle formation increased with increased IM content in the block copolymer. Further consultation with the literature suggested that the observed complexation behavior could be due to the tendency of 1-(4-mercaptobutyl) amidine groups initially formed following reaction of primary amines with 2-IT to cyclize and form N-substituted 2-iminothiolane moieties. The mechanism proposed for N-substituted 2-iminothiolane formation is shown in Figure 7, reproduced from the work of Mokotoff et al. and Singh et al.<sup>16,17</sup> These authors showed that reaction of primary amines with 2-IT resulted in the formation of linear 1-(4-mercaptobutyl) amidine functional groups initially but this species quickly disappeared along with concurrent appearance of cyclic N-substituted 2-iminothiolane structures. This behavior was also observed following the reaction of glucosamine with 2-IT, and the N-substituted 2-iminothiolane structure was confirmed by mass spectrometry.<sup>26</sup> Formation of the N-substituted 2-iminothiolane rings is rapid at room temperature and slightly basic pH, with half-lives of the initially formed 1-(4-mercaptobutyl) amidine  $\sim$ 0.5–3 h, depending on the  $pK_a$  of the amine nucleophile used for reaction with 2-IT. Specifically, the half-life of 1-(4-mercaptobutyl) amidines formed by reaction of 2-IT with amines having a  $pK_a$  of 9.3–9.8 (which is similar to the  $pK_a$  of lysine amines ( $\sim$ 10) used for reaction with 2-IT in this study) is 1.8–2.8 h at pH 8, 25  $^{\circ}$ C.

Formation of the N-substituted 2-iminothiolane derivative in PEG-*b*-PLL(N2IM-IM) results in a five-membered ring structure. Thus, an appropriate amidination reagent must produce a mercaptoalkyl amidine not capable of ring formation. The chemistry contained in DTBP results in a formation of a 1-(3-mercaptopropyl) amidine group that contains only two carbons between the amidine and thiol and will not cyclize due to the instability of a four-membered ring. Modification of PEG-*b*-PLL with DTBP provided a convenient and stable structure for comparison with PEG-*b*-PLL(N2IM-IM).

$^1$ H NMR analysis of PEG-*b*-PLL(N2IM-IM) confirmed that nearly all lysine amines reacted with 2-IT and also provided direct evidence that both cyclic N-substituted 2-iminothiolane and linear 1-(4-mercaptobutyl) amidine groups were present in the product (Figure 2). Generation of the N-substituted 2-iminothiolane has been reported to produce a small upfield shift ( $\sim$ 0.2 ppm) of protons adjacent to the imine nitrogen in the  $^1$ H NMR spectra of small molecules, and this small shift was also observed in the  $^1$ H NMR spectrum of PEG-*b*-PLL(N2IM-IM).<sup>16</sup> The main peak at 3.25 ppm corresponds to lysine  $\epsilon$ -CH<sub>2</sub> protons adjacent to N-substituted 2-iminothiolane containing side chains and the shoulder at 3.4 ppm corresponds to lysine  $\epsilon$ -CH<sub>2</sub> protons adjacent to 1-(4-mercaptobutyl) amidine containing side chains. Estimation of the ratio of the two side chain structures from

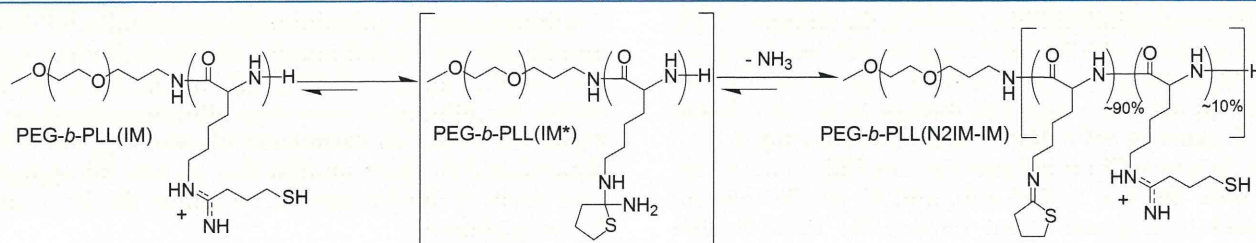


**Figure 7.** Intramolecular rearrangement of 1-(4-mercaptobutyl) amidine groups in PEG-*b*-PLL(IM) into N-substituted 2-iminothiolane moieties in PEG-*b*-PLL(N2IM-IM) via a tetrahedral intermediate structure. Adopted from Singh et al. and Mokotoff et al. (refs 16 and 17). Residual unmodified lysines are not shown in the chemical structures.

integration values showed that the N-substituted 2-iminothiolane ring is the predominant product following reaction with 2-IT (~75%). It should be noted that reaction of PEG-*b*-PLL with 1 molar equiv of 2-IT resulted in only ~60% conversion of lysine amines despite long (18 h) reaction time (data not shown). Reaction with at least a 2-fold excess of 2-IT is essential to achieve ~100% modification of lysine primary amines under the conditions described here. This is likely due to ammonia generated upon formation of N-substituted 2-iminothiolane rings competing for reaction with 2-IT and thus decreasing lysine amine conversion.

In our previous report, we obtained a product that did not show any N-substituted 2-iminothiolane functionality in the <sup>1</sup>H NMR spectrum of isolated polymer product, even at high lysine conversion (see Supporting Information). However, the siRNA complexation behavior at pH 7.4 was nearly identical between the PEG-*b*-PLL(IM) obtained in our previous report and the PEG-*b*-PLL(N2IM-IM) obtained in the current study. We found that treatment of PEG-*b*-PLL(IM) from the previous study with DTT at pH 7.4, and subsequent purification by dialysis, resulted in formation of the N-substituted 2-iminothiolane structures observed in this work (see Supporting Information). Thus, even if N-substituted 2-iminothiolane structures are not observed in the <sup>1</sup>H NMR spectrum of product obtained following reaction of PEG-*b*-PLL with 2-IT (at amounts targeting complete conversion of lysines), the ring structures will form upon reduction with DTT in aqueous buffer at pH 7.4. This seems reasonable if the isolated product contains a high degree of disulfide cross-linking, which would prevent the formation of N-substituted 2-iminothiolane rings. Disulfide formation during the reaction of PEG-*b*-PLL with 2-IT is likely why a residual amount of 1-(4-mercaptobutyl) amidine functionality is observed in the polymer product obtained in this study. It should be noted, however, that the structure of functional groups contained in PEG-*b*-PLL lysine side chains following reaction with lower molar ratios of 2-IT may be more complicated. Residual unmodified lysine amines can react with the N2IM structure to generate N,N'-disubstituted amidines, resulting in cross-linked (inter- or intramolecular) lysine side chains.<sup>27</sup> Thus, for simplicity, we targeted complete conversion of lysine amines with 2-IT in this study.

Formation of the N-substituted 2-iminothiolane derivative in PEG-*b*-PLL(N2IM-IM) product was also evidenced by analysis of free thiol content using Ellman's assay, as this cyclic moiety lacks sulfhydryl groups. Free thiol content was much lower for PEG-*b*-PLL(N2IM-IM) compared to PEG-*b*-PLL(MPA), confirming that the majority of modified lysines contained closed ring structures (Table 1). However, a finite amount (~10% of original lysine side chains) of free thiol was detected in PEG-*b*-PLL(N2IM-IM). This residual thiol content allows for the desired ability to form disulfide cross-links in the core of micelles prepared with PEG-*b*-PLL(N2IM-IM) and siRNA.

Polymeric micelles formed spontaneously upon mixing polymer and siRNA solutions in HEPES buffer (pH 7.4) at room temperature (22 °C). Complexation of block copolymer with siRNA was expressed as a function of the molar ratio of polymer/siRNA. We chose this format because of the complexity of the PEG-*b*-PLL(N2IM-IM) side chain structure, which makes exact definition of charge ratio difficult. Another method commonly used to express the polycation/nucleic acid ratio is N/P ratio. In this case, N typically represents the molar equivalent of amines (+ charge) and P represents the molar equivalents of siRNA phosphates (− charge). For polycations used in this study, the

polymer/siRNA molar ratio is nearly interchangeable with N/P ratio if the charge is retained (i.e., PEG-*b*-PLL(MPA)), as the GL3 siRNA carries a net charge of (−) 40 and the PLL segment in the polycation block of PEG-*b*-PLL contains 46 units. This degree of polymerization for PLL was targeted so that one polymer chain neutralizes the charge of one siRNA molecule.

In general, modification of PEG-*b*-PLL with either 2-IT or DTBP improved the quality (controlled size and PDI) of micelles formed with siRNA. PEG-*b*-PLL alone formed large particles (~200 nm, PDI = 0.4) with siRNA near stoichiometric molar ratios (Table 1). Micelle formation behavior between PEG-*b*-PLL(N2IM-IM) or PEG-*b*-PLL(MPA) and siRNA at pH 7.4 was markedly different. PEG-*b*-PLL(N2IM-IM) formed micelles over a broader range of polymer/siRNA molar ratios (~2–7.6) while micelles formed with PEG-*b*-PLL(MPA) only near stoichiometric molar ratios, with light scattering and fluorescence quenching results in good agreement (Figure 3A and 3C). Micelles formed at the polymer/siRNA molar ratio corresponding to the highest SLI value for both polymers were narrowly dispersed spherical structures as evidenced by the low PDI value obtained in DLS measurement (Table 1) and also by direct TEM observation (Figure 4). Excess polycation inhibited micelle formation in the case of PEG-*b*-PLL(MPA), as the SLI decreased and Cy3-siRNA fluorescence recovered at polymer/siRNA molar ratios above ~1.4 (Figure 3A,C). PEG-*b*-PLL(MPA) retains positive charge due to basic amidine groups (pK<sub>a</sub>~11–12) and rearrangement of side chains into N-substituted 2-iminothiolane structures with a lower pK<sub>a</sub> is prevented due to the shorter methylene spacer between the amidine and thiol.<sup>28</sup> The fact that micelles remain present in complexation mixtures containing a molar excess of PEG-*b*-PLL(N2IM-IM) suggests that this polymer is less charged than PEG-*b*-PLL(MPA), which is expected due to the prevalence of imines with a lower pK<sub>a</sub>. Residual 1-(4-mercaptobutyl) amidine groups (which contain amidine functionality and thus positive charge) as well as unreacted lysine amines in PEG-*b*-PLL(N2IM-IM) likely provide the driving force for polymer association with siRNA through long-range Coulombic interactions. After polymer chains assemble in close proximity, additional short-range non-ionic interactions (van der Waals, dipole–dipole, H-bonding) may occur to further stabilize the structure. When the residual charge of PEG-*b*-PLL(N2IM-IM) is considered (~5% unreacted lysines determined by <sup>1</sup>H NMR and 11% residual 1-(4-mercaptobutyl) amidines determined by Ellman's assay), a ± charge ratio of ~1.4 is calculated at the polymer/siRNA molar ratio of 7.6, where maximum SLI is observed. Assuming that all modified PLL side chains are charged in PEG-*b*-PLL(MPA), the polymer/siRNA molar ratio that resulted in maximum SLI corresponds to a ± ratio of 1.3. Thus, the ± charge ratio corresponding to maximum SLI were nearly the same for both PEG-*b*-PLL(N2IM-IM) and PEG-*b*-PLL(MPA) polymers at pH 7.4.

The effect of N-substituted 2-iminothiolane ring structures on block copolymer complexation with siRNA was confirmed by lowering the pH of complexation solutions. Formation of N-substituted 2-iminothiolane groups results in the loss of highly basic amidine groups and concurrent formation of imines of lower pK<sub>a</sub>. For example, the pK<sub>a</sub> value reported for an imine group contained in a N-substituted 2-iminothiolane formed by reaction of 2-IT with ethanolamine is reported as 6.7, which would result in a drastic loss of charge at pH 7.4 compared to the parent amidine.<sup>16</sup> At acidic complexation conditions

PEG-*b*-PLL(N2IM-IM) and PEG-*b*-PLL(MPA) behaved similarly, with micelles forming only at polymer/siRNA molar ratios near the stoichiometric region (Figure 3B). At pH 5.0, the imine groups of PEG-*b*-PLL(N2IM-IM) were protonated and, thus, cationic nature was restored, which in turn aligned the complexation behavior to that observed with PEG-*b*-PLL(MPA). Interestingly, although protonation of imines altered micelle formation behavior between PEG-*b*-PLL(N2IM-IM) and siRNA, incubation of cross-linked micelles (following disulfide reduction at pH 7.4) at pH 4.0 did not disrupt the micelle structure even at 150 mM NaCl (see Supporting Information). This treatment resulted in micelle swelling, but not micelle disruption.

Results with PEG-*b*-PLL(MPA) as well as protonated PEG-*b*-PLL(N2IM-IM) suggest that excess polycation disrupts micelle formation between block copolymers and siRNA. In the case of PEG-*b*-PLL(N2IM-IM), reduced polymer charge upon formation of N-substituted 2-iminothiolane rings likely reduced electrostatic repulsion between polymer chains and also competition for siRNAs, allowing more polymer to associate with micelle structures. Additionally, PEG-*b*-PLL(N2IM-IM) exhibited maximum fluorescence quenching at a lower polymer/siRNA molar ratio than that corresponding to the maximum SLI value ( $\sim 7.6$ ) and quenching was maintained over the entire range of polymer concentrations tested. This suggests that the polymer significantly interacts with siRNA at polymer/siRNA molar ratios  $\geq 1.8$ , as evidenced by the change in the Cy3 microenvironment leading to quenching. However, polymer association is not complete until polymer:siRNA molar ratios of  $\sim 7.6$ , where maximum SLI was observed. This is consistent with our previous gel retardation studies of micelles prepared with siRNA and PEG-*b*-PLL(N2IM-IM), where siRNA did not enter the gel for complexation solutions prepared at polymer/siRNA ratios  $> 2.7$ .<sup>14</sup>

Micelle *z*-average diameters measured by DLS and micelle core sizes determined by TEM were in good agreement, and the sizes obtained were similar for both PEG-*b*-PLL(N2IM-IM) and PEG-*b*-PLL(MPA) (Table 1 and Figure 4). Low PDI values obtained by DLS measurement of polymer/siRNA assemblies suggests that spherical structures formed, which was confirmed by direct TEM observation of cross-linked micelles. As expected, micelle diameters determined by DLS analysis were larger than the core size of micelles determined from the TEM images. However, the determined size of micelle cores by TEM corroborated well with whole micelle size values observed by DLS, considering the size of PEG and assuming a core-shell micelle structure. The radius of gyration ( $R_g$ ) of PEG 12K in water is 4.68 nm; thus, the tethered PEG chain height is 9.36 nm ( $2 \times R_g$ ) in the so-called mushroom or random coil conformation.<sup>29,30</sup> Addition of the PEG segment length to the measured micelle core size obtained from TEM images results in a calculated diameter of 32.3 nm for PEG-*b*-PLL(N2IM-IM)/siRNA micelles and 35.2 nm for PEG-*b*-PLL(MPA)/siRNA micelles, which are less than the *z*-average values reported in Table 1. Conversion of DLS data to number average diameters directly from the size distribution histogram generated from the ZetaSizer software resulted in a calculated diameter of  $32.0 \pm 2.37$  nm for PEG-*b*-PLL(N2IM-IM)/siRNA micelles and  $32.4 \text{ nm} \pm 1.3$  nm for PEG-*b*-PLL(MPA)/siRNA micelles, which is in excellent agreement with calculated diameters from TEM images (see Supporting Information). Micelle core diameters measured from TEM imaging were smaller for PEG-*b*-PLL(N2IM-IM)/siRNA, while the whole micelle diameter measured by DLS was the same for both PEG-*b*-PLL(N2IM-IM) and PEG-*b*-PLL(MPA). This suggests

that the PEG layer may be thicker in PEG-*b*-PLL(N2IM-IM)/siRNA micelles, where PEG chains become more elongated on the micelle surface due to the close proximity of other chains. This seems reasonable as more polymer may be associating with PEG-*b*-PLL(N2IM-IM)/siRNA micelles, which form in the presence of  $\sim 7.6$  times molar excess of polymer. Altogether, micelle characterization by both DLS and TEM further support that core-shell micelle structures are formed upon association of polymer with siRNA at the polymer:siRNA molar ratio corresponding to maximum SLI.

Modification of PEG-*b*-PLL with 2-IT or DTBP increased the stability of PIC micelles formed with siRNA as evidenced by the maintenance of micelle structures formed with both block copolymers up to 300 mM NaCl (Figure 3D), whereas non-cross-linked assemblies (but not necessarily individual polycation complexes) formed between siRNA and PEG-*b*-PLL nearly completely dissociate in 150 mM NaCl.<sup>14</sup> However, PEG-*b*-PLL(N2IM-IM)/siRNA micelles were ultimately more stable than PEG-*b*-PLL(MPA)/siRNA micelles at high NaCl concentration (600 mM). This suggests that nonionic interactions, such as van der Waals, ion-dipole, or H-bonding (via imine nitrogens) may also contribute to micelle stability. Incubation of PEG-*b*-PLL(N2IM-IM)/siRNA micelles in a high ionic strength solution under reductive conditions resulted in disruption of micelle structures ( $\sim 20\%$  decrease in SLI compared to nonreductive conditions), showing that disulfide cross-links did in fact contribute to micelle stability.

For PEG-*b*-PLL(MPA), dissociation of micelles at high NaCl concentration in the absence of DTT suggests that disulfide cross-linking alone did not provide the same stability provided by PEG-*b*-PLL(N2IM-IM), which had a much lower thiol content and disulfide formation efficiency in the micelle core. However, the degree of intermolecular vs intramolecular disulfide cross-linking in PEG-*b*-PLL(MPA)/siRNA micelles is unknown, and only the former would result in increased micelle stability in the absence of disulfide reducing agents. Micelles formed with PEG-*b*-PLL(MPA) were more sensitive to dissociation in the presence of DTT, indicating that disulfide cross-linking was more critical to improving the stability of micelles prepared solely from electrostatic interactions.

In vitro gene silencing activity of siRNA was improved upon encapsulation within polymeric micelle carriers prepared from PEG-*b*-PLL(N2IM-IM) or PEG-*b*-PLL(MPA), as no gene silencing was observed for naked siRNA or PEG-*b*-PLL particles (Figure 5 and Table 1). Gene silencing was highest for PEG-*b*-PLL(MPA)/siRNA micelles, which may be attributed to higher sensitivity to disulfide reduction. PEG-*b*-PLL(MPA)/siRNA micelles likely dissociate more readily once internalized into cells, thus, releasing the siRNA cargo. This is consistent with the observed difference in lag time before gene silencing, where PEG-*b*-PLL(MPA)/siRNA micelles showed gene silencing after only 10 h and PEG-*b*-PLL(N2IM-IM)/siRNA micelles showed gene silencing after 25 h. More stable PEG-*b*-PLL(N2IM-IM) micelles likely dissociate and release siRNA more slowly, thus, requiring more time before gene knockdown is observed. Nonetheless, the fact that gene silencing was observed after 55 h of incubation indicates that both micelle structures were effective at protecting siRNA from degradation into inactive fragments within the cell culture medium or off-target sites within the subcellular environment.

One of our goals regarding development of a siRNA delivery system is to produce a carrier that has prolonged residence time

in the bloodstream, allowing the carrier to be administered by I.V. injection. Polymer/siRNA micelle structures obtained in this study are particularly attractive candidates for cancer treatment by I.V. injection as they are large enough to escape rapid renal filtration ( $\sim 10$  nm cutoff) but small enough ( $<100$  nm) to gain tumor mass accumulation by the enhanced permeability and retention (EPR) effect.<sup>31,32</sup> Thus, we investigated the blood circulation time of micelles prepared in this work. In order to have prolonged blood circulation the carrier must not interact with blood components (leading to aggregation or micelle dissociation) and must also remain intact to protect siRNA from premature release and degradation. Blood circulation results clearly identify that micelles prepared with PEG-*b*-PLL(N2IM-IM) and siRNA remain in the bloodstream longer than any other formulation tested (Figure 6A). Micelles prepared with PEG-*b*-PLL(MPA) provided some improvement in blood residence time compared to naked siRNA and PEG-*b*-PLL/siRNA particles. This result suggests that even a high degree of disulfide cross-linking was insufficient to greatly prolong residence time in the bloodstream. However, although disulfide formation efficiency was high for PEG-*b*-PLL(MPA)/siRNA micelles, the amount of intermolecular cross-linking is unknown. A longer spacer between the amidine and thiol in modified PLL side-chains may further improve micelle stability and blood residence time.

Improved blood circulation for PEG-*b*-PLL(N2IM-IM)/siRNA micelles may not be solely linked to micelle stability. As mentioned previously, the PEG density is likely higher for micelles formed with PEG-*b*-PLL(N2IM-IM) than those prepared with PEG-*b*-PLL(MPA) as the former were prepared at a higher molar ratio of polymer. Higher PEG density may further reduce nonspecific interactions of micelles with blood components leading to longer circulation time. The impact of PEG density on stability in the blood compartment is beyond the scope of this study but we hope to clarify this in the future. Furthermore, the lower charge density of PEG-*b*-PLL(N2IM-IM) likely results in diffuse charges in the micelle core which in turn could reduce interactions with charged (mainly anionic) components in the bloodstream.

In addition to providing the longest blood circulation time, micelles prepared with PEG-*b*-PLL(N2IM-IM) also showed the lowest increase in tissue fluorescence outside of blood vessels. Extravasation into surrounding tissues suggests that micelle structures dissociated and fluorescent labeled siRNA was released and possibly degraded, producing small fragments of siRNA with high tissue permeability. We have previously observed such effects with fluorescein and fluorescein-labeled dextrans. In that study, we observed that free dye and dye-labeled dextrans lower than  $\sim 10$  kDa quickly entered the tissue following I.V. injection, whereas higher MW dye-labeled dextrans did not.<sup>21</sup> Thus reduced migration of Cy5 fluorescence into the tissue region surrounding blood vessels in the case of PEG-*b*-PLL(N2IM-IM)/siRNA micelles provides further evidence that micelles remained intact in the bloodstream.

In summary, we found that a highly charged cationic block copolymer was not necessary to form micellar structures with siRNA. PEG-*b*-PLL(N2IM-IM) formed micelles with siRNA despite loss of a large percentage of charged amidine groups. This block copolymer likely retained enough residual charge to interact with siRNA and assemble into higher-ordered micellar structures but not so much charge as to electrostatically repel itself at high polymer concentrations. The unique association behavior of PEG-*b*-PLL(N2IM-IM) and siRNA represents a nontraditional

PIC assembly where the polycation contains low charge density and micelles form in the presence of excess block copolymer. In this regard, PEG-*b*-PLL(N2IM-IM)/siRNA micelles are attractive from a practical point of view because micelle formation is less sensitive to slight variations in polymer concentration. In contrast, strongly charged PEG-*b*-PLL(MPA) cationic block copolymer showed very sensitive micelle formation behavior with siRNA and excess polycation inhibited micelle assembly. Inhibition of micelle formation was likely due to repulsion of charged polymer chains and increased competition with siRNAs. As a result, preparation of micelles with PEG-*b*-PLL(MPA) and siRNA required careful control of polymer and siRNA mixing ratios.

Covalent disulfide cross-linking is expected to improve micelle stability compared to particles prepared from unmodified PEG-*b*-PLL, but a high thiol-content block copolymer did not produce the most stable micelle structure in this work. Micelles prepared from polymer comprising relatively low free thiol content were more resistant to dissociation *in vitro* and also exhibited longer residence time in the bloodstream *in vivo*. The possibility of noncovalent interactions between polymer chains in addition to covalent disulfide cross-linking greatly improved micelle stability. Improved micelle stability came at a performance cost, as noncovalent polymer interactions in addition to covalent disulfide cross-links reduced the sensitivity of micelles to disruption under disulfide reducing conditions. Increased stability and reduced sensitivity to disulfide reduction were likely responsible for the increased lag-time observed for the onset of gene silencing in cell culture experiments. On the other hand, the benefit of preparing stable micelles with high polymer content was realized *in vivo*. Micelles prepared with PEG-*b*-PLL(N2IM-IM) exhibited longer blood circulation, which is necessary for I.V. administration of siRNA delivery systems. Thus, the chemistry contained in the block copolymer must be carefully controlled to produce effective siRNA carriers on the cellular and whole organism level.

Understanding the mechanisms that govern the assembly and stability of nanoparticles is crucial for improvements of their design. The findings of this work may be further generalized in the sense that “soft” polycations containing less positive charge and “hard” polycations with high charge density differ in their complexation behavior with siRNA. While interactions between polyelectrolytes can provide the driving force for particle assembly, the stability of the resulting polyplex may be further enhanced by contributions from nonionic interactions in addition to covalent cross-links to form more robust structures. Formation of micelle structures between polymers and siRNA may be more sensitive to the chemistries contained in the polymer component than large polyanions such as plasmid DNA (pDNA). siRNA is much smaller than pDNA and cannot condense and adopt different conformations in response to excess polycation. Instead, siRNA can simply dissociate from the polyion complex due to the increased mobility of a shorter polyanion. Preparation of stable siRNA polymeric micelle nanocarriers is hinged on a delicate balance of chemistries contained in the polymer component.

## CONCLUSIONS

In this work, we found that a high degree of PEG-*b*-PLL modification with 2-iminothiolane resulted in the formation of N-substituted 2-iminothiolane structures in the majority of reacted lysine side chains. This chemistry reduced the polymer charge density at pH 7.4, which in turn shifted the optimal conditions of micelle formation to favor higher molar ratios of

polymer/siRNA compared to a highly charged block copolymer. Despite lower free thiol content and disulfide cross-linking efficiency, micelles formed with PEG-*b*-PLL(N2IM-IM) and siRNA were more stable in buffer and in the bloodstream compared to those formed with PEG-*b*-PLL(MPA) and siRNA. These results highlight the importance of nonionic and non-covalent interactions toward the stability of micelles formed between siRNA and block copolymers. However, higher micelle stability and loss of sensitivity to disulfide reducing conditions resulted in lower siRNA activity on the cellular level; thus, reversible micelle stability is critical to achieve high gene silencing at the target site. The siRNA encapsulating micelles described in this work are promising candidates as carriers for siRNA delivery applications and our efforts to correlate micelle properties with in vitro and in vivo efficacy are ongoing.

## ■ ASSOCIATED CONTENT

**S Supporting Information.** Figures showing (1) a summary of scattered light intensity, size, and PDI of micelles (non-cross-linked) contained in PEG-*b*-PLL(N2IM-IM)/siRNA solutions at various polymer concentrations, (2) scattered light intensity, size, and PDI of PEG-*b*-PLL(N2IM-IM) polymer solutions at pH 7.4 and 4.0, (3) scattered light intensity of cross-linked PEG-*b*-PLL(N2IM-IM) micelles at pH 7.4 and pH 4.0 at various micelle concentrations, (4) size distribution histograms of cross-linked micelles determined by DLS, (5) <sup>1</sup>H NMR analysis of PEG-*b*-PLL(IM) following reduction in DTT at pH 7.4, (6) cytotoxicity of polymer/siRNA micelles prepared with PEG-*b*-PLL(N2IM-IM) and PEG-*b*-PLL(MPA), and (7) blood circulation profile of cross-linked micelles in different mice (*n* = 2) are provided. This material is available free of charge via the Internet at <http://pubs.acs.org>.

## ■ AUTHOR INFORMATION

### Corresponding Author

\*Tel.: +81-3-5841-7138. Fax: +81-3-5841-7139. E-mail: [kataoka@bmw.t.u-tokyo.ac.jp](mailto:kataoka@bmw.t.u-tokyo.ac.jp).

## ■ ACKNOWLEDGMENT

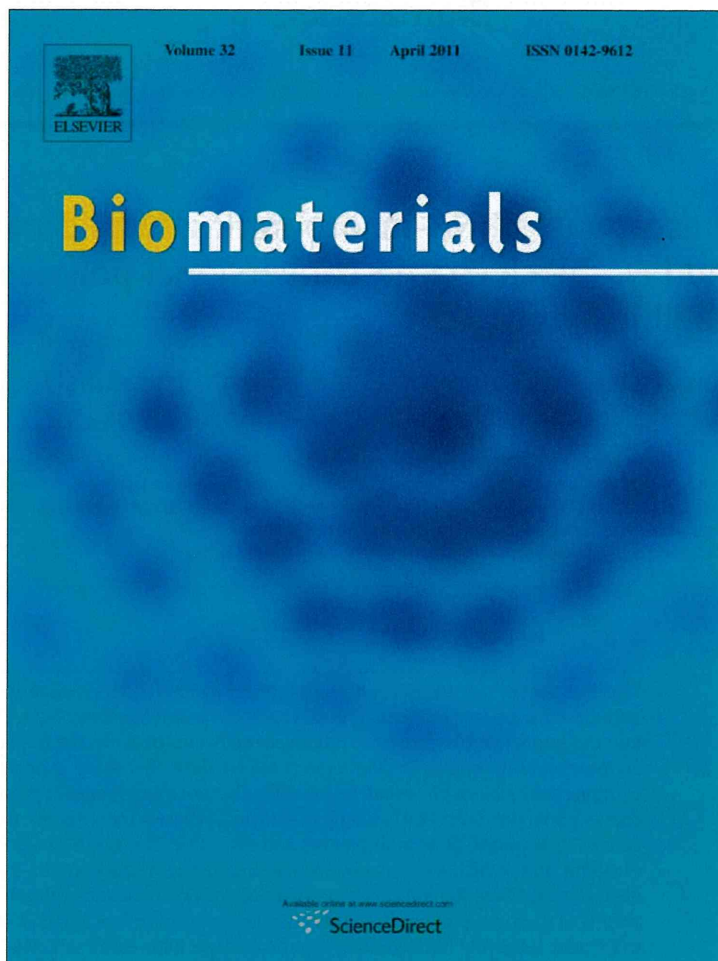
This research was financially supported by the Funding Program for World-Leading Innovative R&D in Science and Technology (FIRST), the Japan Society for the Promotion of Science (JSPS), and the Core Research Program for Evolutional Science and Technology (CREST) from the Japan Science and Technology Agency (JST).

## ■ REFERENCES

- (1) Whitehead, K.; Langer, R.; Anderson, D. *Nat. Rev. Drug Discovery* **2009**, *8*, 129–138.
- (2) Gary, D.; Puri, N.; Won, Y. *J. Controlled Release* **2007**, *121*, 64–73.
- (3) Juliano, R.; Alam, M.; Dixit, V.; Kang, H. *Nucleic Acids Res.* **2008**, *36*, 4158–4171.
- (4) Ai, H.; Jones, S.; Lvov, Y. *Cell Biochem. Biophys.* **2003**, *39*, 23–43.
- (5) Hammond, P. *Adv. Mater.* **2004**, *16*, 1271–1293.
- (6) Christie, R.; Nishiyama, N.; Kataoka, K. *Endocrinology* **2010**, *151*, 466–473.
- (7) Wang, Y.; Angelatos, A.; Caruso, F. *Chem. Mater.* **2008**, *20*, 848–858.
- (8) Mintzer, M.; Simanek, E. *Chem. Rev.* **2009**, *109*, 259–302.

- (9) Meyer, M.; Philipp, A.; Oskuee, R.; Schmidt, C.; Wagner, E. *J. Am. Chem. Soc.* **2008**, *130*, 3272–3273.
- (10) Lee, Y.; Miyata, K.; Oba, M.; Ishii, T.; Fukushima, S.; Han, M.; Koyama, H.; Nishiyama, N.; Kataoka, K. *Angew. Chem., Int. Ed.* **2008**, *47*, 5163–5166.
- (11) Convertine, A.; Benoit, D.; Duvall, C.; Hoffman, A.; Stayton, P. *J. Controlled Release* **2009**, *133*, 221–229.
- (12) Takae, S.; Miyata, K.; Oba, M.; Ishii, T.; Nishiyama, N.; Itaka, K.; Yamasaki, Y.; Koyama, H.; Kataoka, K. *J. Am. Chem. Soc.* **2008**, *130*, 6001–6009.
- (13) Miyata, K.; Kakizawa, Y.; Nishiyama, N.; Harada, A.; Yamasaki, Y.; Koyama, H.; Kataoka, K. *J. Am. Chem. Soc.* **2004**, *126*, 2355–2361.
- (14) Matsumoto, S.; Christie, R.; Nishiyama, N.; Miyata, K.; Ishii, A.; Oba, M.; Koyama, H.; Yamasaki, Y.; Kataoka, K. *Biomacromolecules* **2009**, *10*, 119–127.
- (15) Meister, A.; Anderson, M. *Annu. Rev. Biochem.* **1983**, *52*, 711–760.
- (16) Singh, R.; Kats, L.; Blattler, W.; Lambert, J. *Anal. Biochem.* **1996**, *236*, 114–125.
- (17) Mokotoff, M.; Mocarski, Y.; Gentsch, B.; Miller, M.; Zhou, J.; Chen, J.; Ball, E. *J. Pept. Res.* **2001**, *57*, 383–389.
- (18) Harada, A.; Kataoka, K. *Macromolecules* **1995**, *28*, 5294–5299.
- (19) Ellman, G. *Arch. Biochem. Biophys.* **1959**, *82*, 70–77.
- (20) Tam, J. P.; Wu, C. R.; Liu, W.; Zhang, J. W. *J. Am. Chem. Soc.* **1991**, *113*, 6657–6662.
- (21) Matsumoto, Y.; Nomoto, T.; Cabral, H.; Matsumoto, Y.; Watanabe, S.; Christie, R. J.; Miyata, K.; Oba, M.; Ogura, T.; Yamasaki, Y.; Nishiyama, N.; Yamasoba, T.; Kataoka, K. *Biom. Opt. Express* **2010**, *1*, 1209–1216.
- (22) Browne, D.; Kent, S. *Biochem. Biophys. Res. Commun.* **1975**, *67*, 126–132.
- (23) Gruber, H.; Hahn, C.; Kada, G.; Riener, C.; Harms, G.; Ahrer, W.; Dax, T.; Knaus, H. *Bioconjugate Chem.* **2000**, *11*, 696–704.
- (24) Berlier, J.; Rothe, A.; Buller, G.; Bradford, J.; Gray, D.; Filanoski, B.; Telford, W.; Yue, S.; Liu, J.; Cheung, C.; Chang, W.; Hirsch, J.; Beechem, J.; Haugland, R. *J. Histochem. Cytochem.* **2003**, *51*, 1699–1712.
- (25) Anbazhagan, V.; Kathiravan, A.; Jhonsi, M.; Renganathan, R. Z. *Phys. Chem.* **2007**, *221*, 929–939.
- (26) Kafedjiiski, K.; Krauland, A.; Hoffer, M.; Bernkop-Schnurch, A. *Biomaterials* **2005**, *26*, 819–826.
- (27) Hahn, F.; Mullen, K.; Schepers, U. *Synlett* **2008**, *18*, 2785–2790.
- (28) Koppel, I.; Koppel, J.; Leito, I.; Green, L. *J. Phys. Org. Chem.* **1996**, *9*, 265–268.
- (29) Kawaguchi, S.; Imai, G.; Suzuki, J.; Miyahara, A.; Kitano, T. *Polymer* **1997**, *38*, 2885–2891.
- (30) Kenausis, G.; Voros, J.; Elbert, D.; Huang, N.; Hofer, R.; Ruiz-Taylor, L.; Textor, M.; Hubbell, J.; Spencer, N. *J. Phys. Chem. B* **2000**, *104*, 3298–3309.
- (31) Choi, H.; Liu, W.; Misra, P.; Tanaka, E.; Zimmer, J.; Ipe, B.; Bawendi, M.; Frangioni, J. *Nat. Biotechnol.* **2007**, *25*, 1165–1170.
- (32) Maeda, H.; Wu, J.; Sawa, T.; Matsumura, Y.; Hori, K. *J. Controlled Release* **2000**, *65*, 271–284.

Provided for non-commercial research and education use.  
Not for reproduction, distribution or commercial use.



This article appeared in a journal published by Elsevier. The attached copy is furnished to the author for internal non-commercial research and education use, including for instruction at the authors institution and sharing with colleagues.

Other uses, including reproduction and distribution, or selling or licensing copies, or posting to personal, institutional or third party websites are prohibited.

In most cases authors are permitted to post their version of the article (e.g. in Word or Tex form) to their personal website or institutional repository. Authors requiring further information regarding Elsevier's archiving and manuscript policies are encouraged to visit:

<http://www.elsevier.com/copyright>



Contents lists available at ScienceDirect

Biomaterials

journal homepage: [www.elsevier.com/locate/biomaterials](http://www.elsevier.com/locate/biomaterials)

## Enhanced endosomal escape of siRNA-incorporating hybrid nanoparticles from calcium phosphate and PEG-block charge-conversional polymer for efficient gene knockdown with negligible cytotoxicity

Frederico Pittella<sup>a</sup>, Mingzhen Zhang<sup>b,d</sup>, Yan Lee<sup>b,e</sup>, Hyun J. Kim<sup>b</sup>, Theofilus Tockary<sup>b</sup>, Kensuke Osada<sup>b</sup>, Takehiko Ishii<sup>a</sup>, Kanjiro Miyata<sup>c</sup>, Nobuhiro Nishiyama<sup>c</sup>, Kazunori Kataoka<sup>a,b,c,\*</sup>

<sup>a</sup> Department of Bioengineering, Graduate School of Engineering, The University of Tokyo, 7-3-1 Hongo, Bunkyo-ku, Tokyo 113-8656, Japan

<sup>b</sup> Department of Materials Engineering, Graduate School of Engineering, The University of Tokyo, 7-3-1 Hongo, Bunkyo-ku, Tokyo 113-8656, Japan

<sup>c</sup> Center for Disease Biology and Integrative Medicine, Graduate School of Medicine, The University of Tokyo, 7-3-1 Hongo, Bunkyo-ku, Tokyo 113-0033, Japan

<sup>d</sup> School of Ophthalmology and Optometry, Wenzhou Medical College, Wenzhou, Zhejiang 325027, PR China

<sup>e</sup> Department of Chemistry, College of Natural Science, Seoul National University, Seoul 151-747, Republic of Korea

### ARTICLE INFO

#### Article history:

Received 4 December 2010

Accepted 31 December 2010

Available online 26 January 2011

#### Keywords:

Calcium phosphate nanoparticles

Endosomal escape

Vascular endothelial growth factor (VEGF)

siRNA

Charge-conversional polymer (CCP)

Poly(ethylene glycol) (PEG)

### ABSTRACT

Development of safe and efficient short interfering RNA (siRNA) delivery system for RNA interference (RNAi)-based therapeutics is a current critical challenge in drug delivery field. The major barriers in siRNA delivery into the target cytoplasm are the fragility of siRNA in the body, the inefficient cellular uptake, and the acidic endosomal entrapment. To overcome these barriers, this study is presenting a hybrid nanocarrier system composed of calcium phosphate comprising the block copolymer of poly(ethylene glycol) (PEG) and charge-conversional polymer (CCP) as a siRNA vehicle. In these nanoparticles, the calcium phosphate forms a stable core to incorporate polyanions, siRNA and PEG–CCP. The synthesized PEG–CCP is a non-toxic endosomal escaping unit, which induces endosomal membrane destabilization by the produced polycation through degradation of the flanking *cis*-aconitylamide of CCP in acidic endosomes. The nanoparticles prepared by mixing of each component was confirmed to possess excellent siRNA-loading efficiency (~80% of dose), and to present relatively homogenous spherical shape with small size. With negligible cytotoxicity, the nanoparticles efficiently induced vascular endothelial growth factor (VEGF) mRNA knockdown (~80%) in pancreatic cancer cells (PanC-1). Confocal laser scanning microscopic observation revealed rapid endosomal escape of siRNA with the nanoparticles for the excellent mRNA knockdown. The results obtained demonstrate our hybrid nanoparticle as a promising candidate to develop siRNA therapy.

© 2011 Elsevier Ltd. All rights reserved.

### 1. Introduction

Since the finding of RNA interference (RNAi) in 1998 [1], the scientific community has experienced the excitement to develop a new research field. Short interfering RNA (siRNA), which allows the cleavage of the complementary mRNA for the reduced protein production in mammalian cells, provided new perspectives for potential treatment of intractable and genetic related diseases [2]. With the decoding of the human genome [3–5], it has become possible to aim a great variety of genes involved in key pathways of physiopathologies. However, a safe and efficient delivery of siRNA into the target cytoplasm has still been a major challenge. Naked

siRNAs are susceptible to enzymatic degradation in the body and also possess large size (~13 kDa) and anionic charges suppressing the penetration into cellular membrane [6], thus requiring carrier systems to overcome these barriers.

Calcium phosphate (CaP) precipitates were used as transfection reagents of viral DNA for the first time in early 1970s [7], as they are believed to be non-toxic based on homology to natural inorganic materials such as teeth and bones. Notably, CaP precipitates can bind and encapsulate polyanions/nucleic acids by an easy and inexpensive method to protect the nucleic acids from enzymatic degradation and to deliver into cells. However, one of their major limitations is the uncontrollable rapid growth of calcium phosphate crystal after preparation, resulting in the formation of large agglomerates (>μm) to appreciably reduce the transfection efficiency [8–10]. In this regard, our previous studies have addressed poly(ethylene glycol) (PEG)-coating of CaP precipitates utilizing PEG–polyanion block copolymers [9,11–14]. Hydrophilic and neutral PEG is widely known

\* Corresponding author. Department of Bioengineering, Graduate School of Engineering, The University of Tokyo, 7-3-1 Hongo, Bunkyo-ku, Tokyo 113-8656, Japan.

E-mail address: [kataoka@bmvw.t.u-tokyo.ac.jp](mailto:kataoka@bmvw.t.u-tokyo.ac.jp) (K. Kataoka).

to provide a nanoparticle with excellent colloidal stability as well as reduced protein adsorption and immunogenicity [15–17]. Indeed, the integration of PEG-block polyanions, such as poly(aspartic acid) (PAsp) [9,12], poly(methacryl acid) [13], and siRNA [14], into CaP precipitates led to the formation of size-controllable hybrid nanoparticles with PEG palisade, which appreciably facilitated the internalization of nucleic acids by cells.

Herein, we considered the next challenge in the CaP carriers as the endosomal escape, since they are usually internalized by cells through endocytosis pathway to be delivered into acidic endosome or lysosome, resulting in enzymatic degradation of the payload nucleic acids [18]. Toward the endosomal escape with polymeric materials, our previous studies have reported a cationic polyaspartamide with a 1,2-diaminoethane side chain (poly[*N*-[*N'*-(2-aminoethyl)-2-aminoethyl]aspartamide], PAsp(DET)) to exert strong membrane destabilization selectively in acidic endosomal compartments for efficient endosomal escape with low cytotoxicity [19–22]. Note that PAsp(DET) possesses two unique advantages for its excellent transfection: 1) the pH-selective membrane destabilization based on the distinctive two step protonation behavior in the side chain, i.e., mono-protonated form with minimal membrane damages at neutral pH and di-protonated form exerting strong membrane disruption at acidic pH [20]; 2) the spontaneous biodegradability based on the selective backbone cleavage even under physiological conditions [21].

In this work, in order to improve the endosomal escape as well as the colloidal stability of CaP precipitates, a block copolymer of PEG and an endosomal escaping polymer was synthesized and integrated into the CaP nanoparticles incorporating siRNA. Indeed, we modified the flanking primary amines of PEG-PAsp(DET) with *cis*-aconitic anhydride [23,24] to convert the cationic charges to net negative ones with two carboxylates of the *cis*-aconityl moiety (PEG-poly[*N*-[*N'*-(*N''*-*cis*-aconityl-2-aminoethyl)-2-aminoethyl]aspartamide], PEG-PAsp(DET-Aco)) for effective binding to CaP nanoparticles. Noteworthy, the prepared *cis*-aconitylamide shows high stability at neutral and basic pHs but it becomes cleavable at acidic pH to reproduce cationic PAsp(DET) from anionic PAsp(DET-Aco) in endosome/lysosome, which is termed the charge-conversional polymer [23–25]. The hybrid nanoparticle prepared from PEG-PAsp(DET-Aco), siRNA, and CaP does not contain inherent toxic materials, such as polycations, thereby leading to potentially lower toxicity compared to conventional polyplex carriers from polycations and siRNA. Thus, the nanoparticles prepared by simple mixing of each component were physicochemically and biologically characterized by the comparison with non-charge-conversional control polyanions to demonstrate the utility of our hybrid system from the PEG-charge-conversional polymer for siRNA delivery.

## 2. Material and methods

### 2.1. Materials

*cis*-Aconitic anhydride, tricarballic acid, and Dulbecco's modified eagle's medium (DMEM) were purchased from Sigma–Aldrich (St. Louis, MO).  $\alpha$ -Methoxy- $\omega$ -amino-poly(ethylene glycol) (MeO-PEG-NH<sub>2</sub>) ( $M_w$ : 12,000) and  $\beta$ -benzyl-L-aspartate *N*-carboxyanhydride (BLA-NCA) were obtained from NOF Co, Inc. (Tokyo, Japan) and Chuo Kaseihin Co., Inc. (Tokyo, Japan), respectively. *N*-Methyl-2-pyrrolidone (NMP), diethylenetriamine (DET), dimethyl sulfoxide (DMSO), *N,N*-dimethylformamide (DMF), dichloromethane (DCM), and acetic anhydride were purchased from Tokyo Chemical Industry Co. Ltd. (Tokyo, Japan) or Nacalai Tesque (Tokyo, Japan), and used after a conventional distillation. Acetic acid, acetonitrile, acetone, diethyl ether, and hydrochloric acid were purchased from Wako Pure Chemical Industries Ltd. (Osaka, Japan). Fetal bovine serum (FBS) was purchased from Dainippon Sumitomo Pharma Co., Ltd. (Osaka, Japan). The primers for human actin and human VEGF were synthesized by Hokkaido System Science (Hokkaido, Japan) and the sequences are: CCAACCGCAGAGAAGATGA (actin forward); CCAGAGCGCTACAGGGATAG (actin reverse); AGTGGTCCAGGCTGCAC (VEGF forward); TCCATGAACCTCACCACTTCGT (VEGF reverse). All the siRNAs were synthesized by Hokkaido System Science (Hokkaido, Japan) and the sequences of VEGF siRNA (siVEGF) are: 5'-GGAGUACCCUGAU-GAGAUCdTdT-3' (sense); 5'-GAUCUCAUCAGGGUACUCdTdT-3' (antisense), and GL3

luciferase siRNA (siGL3) are: 5'-CUU ACG CUG AGU ACU UCG AdTdT-3' (sense); 5'-UCC AAG UAC UCA GCG UAA GdTdT-3' (antisense).

### 2.2. Synthesis of block copolymer with poly(ethylene glycol) and charge-conversional polymer (PEG-CCP) segments

#### 2.2.1. Synthesis of poly(ethylene glycol)-*b*-poly[*N*-[*N'*-(2-aminoethyl)-2-aminoethyl]aspartamide] (PEG-PAsp(DET))

PEG-PAsp(DET) was prepared as previously reported with slight modification [21]. Briefly, BLA-NCA (780 mg; 3.13 mmol) was dissolved in 0.7 mL of DMF, and then in 7.3 mL of DCM. The polymerization was initiated from the primary amino group of MeO-PEG-NH<sub>2</sub> ( $M_w$  = 12,000, 500 mg; 0.0417 mmol) to obtain PEG-PBLA (1100 mg) as a precursor. Size exclusion chromatography (SEC) was performed to determine the molecular weight distribution ( $M_w/M_n$ ) of the obtained PEG-PBLA using a TOSOH HLC-8220 equipped with TSK gel columns (SuperAW4000 and SuperAW3000  $\times$  2; eluent: NMP with 50 mM LiBr; flow rate: 0.3 mL min<sup>-1</sup>; temperature: 40 °C) and an internal refractive index (RI) detector. The  $M_w/M_n$  was confirmed to be 1.07 from the SEC chart using PEG standards for the  $M_w$  calibration (data not shown). The degree of polymerization of PBLA in PEG-PBLA was determined to be 96 from the peak intensity ratio of the methylene protons of PEG (-OCH<sub>2</sub>CH<sub>2</sub>-,  $\delta$  = 3.5 ppm) to the benzyl protons of PBLA (C<sub>6</sub>H<sub>5</sub>CH<sub>2</sub>-,  $\delta$  = 5.1 and 7.3 ppm) in the <sup>1</sup>H NMR measurement (data not shown). All of the NMR assays were performed using 3-(trimethylsilyl)-3,3,2,2-tetrauteropropionic acid sodium salt *d*<sub>4</sub>-TSPA as an internal standard. Then, PEG-PBLA (100 mg) was dissolved in NMP (2 mL) and cooled at 5 °C. Diethylenetriamine (DET) (3 mL; 100 equiv to benzyl groups of PBLA segment) was diluted with the same volume of NMP, and then the first solution was added and stirred for 4 h at 0 °C (ice bath). The reaction was stopped adding the polymer solution to cold 20% acetic acid (30 mL) drop-by-drop. The neutralized solution was dialyzed against 0.01 M hydrochloric acid solution and then in de-ionized water at 4 °C. As a hydrochloride salt form, a white powder was obtained after lyophilization of the dialyzed solution (91.2 mg, 69.6% yield). The quantitative conversion of the BLA to Asp(DET) was confirmed from the peak intensity ratio of the methylene protons in PEG (-OCH<sub>2</sub>CH<sub>2</sub>-,  $\delta$  = 3.7 ppm) to the ethylene protons in the 1,2-diaminoethane moiety (H<sub>2</sub>N(CH<sub>2</sub>)<sub>2</sub>NH(CH<sub>2</sub>)<sub>2</sub>NH-,  $\delta$  = 2.8–3.4 ppm) in the <sup>1</sup>H NMR spectrum in D<sub>2</sub>O at 50 °C (Supporting Information).

#### 2.2.2. Synthesis of poly(ethylene glycol)-*b*-poly[*N*-[*N'*-(*N''*-*cis*-aconityl-2-aminoethyl)-2-aminoethyl]aspartamide] (PEG-PAsp(DET-Aco))

PEG-PAsp(DET) (17.5 mg, 0.0538 mmol of primary amine) was dissolved in 0.5 M NaHCO<sub>3</sub> at pH 9.1 (50 mL). *cis*-Aconitic anhydride powder (420 mg, 2.69 mmol) was added to the solution slowly and stirred at 0 °C for 2 h. The reaction mixture was purified by centrifugal ultrafiltration with Amicon Ultra (MWCO = 10,000; Millipore (Billerica, MA)) three times with de-ionized water at 4 °C. The final product was obtained as a white powder after lyophilization (14.9 mg, 64.7% yield). The quantitative conversion of primary amines in Asp(DET) side chain to *cis*-aconitylamide was confirmed from the peak intensity ratio of the methine protons in the main chain (-COCH<sub>2</sub>CH(CO-)NH-, -COCH(CH<sub>2</sub>-)NH-,  $\delta$  = 4.8 ppm) to methine protons of the *cis*-aconityl moiety (-COCH(C(COONa)CH<sub>2</sub>COONa),  $\delta$  = 6.0 ppm) in <sup>1</sup>H NMR spectrum in D<sub>2</sub>O at 50 °C (Fig. 1).

### 2.3. Synthesis of block copolymer with poly(ethylene glycol) and non-charge-conversional polymers (PEG-nCCP) segments

#### 2.3.1. Synthesis of carballylic anhydride

Carballylic anhydride was prepared as previously reported [26] with slight modification. Briefly, tricarballic acid (4.4 g, 0.025 mol) was reacted with acetic anhydride (4.73 mL, 0.05 mol) at 45 °C for 1 h. The excess of acetic anhydride was evaporated under reduced pressure. Further, the product was dissolved in the minimum amount of ethyl acetate at 80 °C and filtered. The solution was allowed to stand for 5 h at room temperature and then overnight at 4 °C. The obtained crystal was then vacuum-filtered, washed with excess of diethyl ether, and then dried in vacuum to yield a white crystal (760 mg, 19.2% yield). The reaction was confirmed by <sup>1</sup>H NMR spectrum in acetone at 25 °C (-COCH<sub>2</sub>CH(CH<sub>2</sub>COOH)CO-,  $\delta$  = 2.94, 2.86 ppm), (CH<sub>2</sub>COOH,  $\delta$  = 2.44 ppm) (data not shown).

#### 2.3.2. Synthesis of poly(ethylene glycol)-*b*-poly[*N*-[*N'*-(*N''*-carballylyl-2-aminoethyl)-2-aminoethyl]aspartamide] (PEG-PAsp(DET-Car))

PEG-PAsp(DET) (15 mg, 0.046 mmol of primary amine) was dissolved in 0.5 M NaHCO<sub>3</sub> at pH 9.1 (50 mL). Carballylic anhydride powder (Car) (363 mg, 2.3 mmol) was added to the solution slowly and stirred at 0 °C for 2 h. The reaction mixture was purified by centrifugal ultrafiltration with Amicon Ultra (MWCO = 10,000; Millipore (Billerica, MA)) three times with de-ionized water at 4 °C. The final product was obtained as a white powder after lyophilization (13.5 mg, 68.3% yield). The quantitative conversion of the primary amines in the Asp(DET) side chain to carballylamide was confirmed from the peak intensity ratio of the methine protons in the main chain (-COCH<sub>2</sub>CH(CO-)NH-, -COCH(CH<sub>2</sub>-)NH-,  $\delta$  = 4.8 ppm) to the methylene protons of the carballylyl moiety (-CH<sub>2</sub>CH(COONa)CH<sub>2</sub>COONa,  $\delta$  = 2.5) in the <sup>1</sup>H NMR spectrum in D<sub>2</sub>O at 50 °C (Supporting Information).

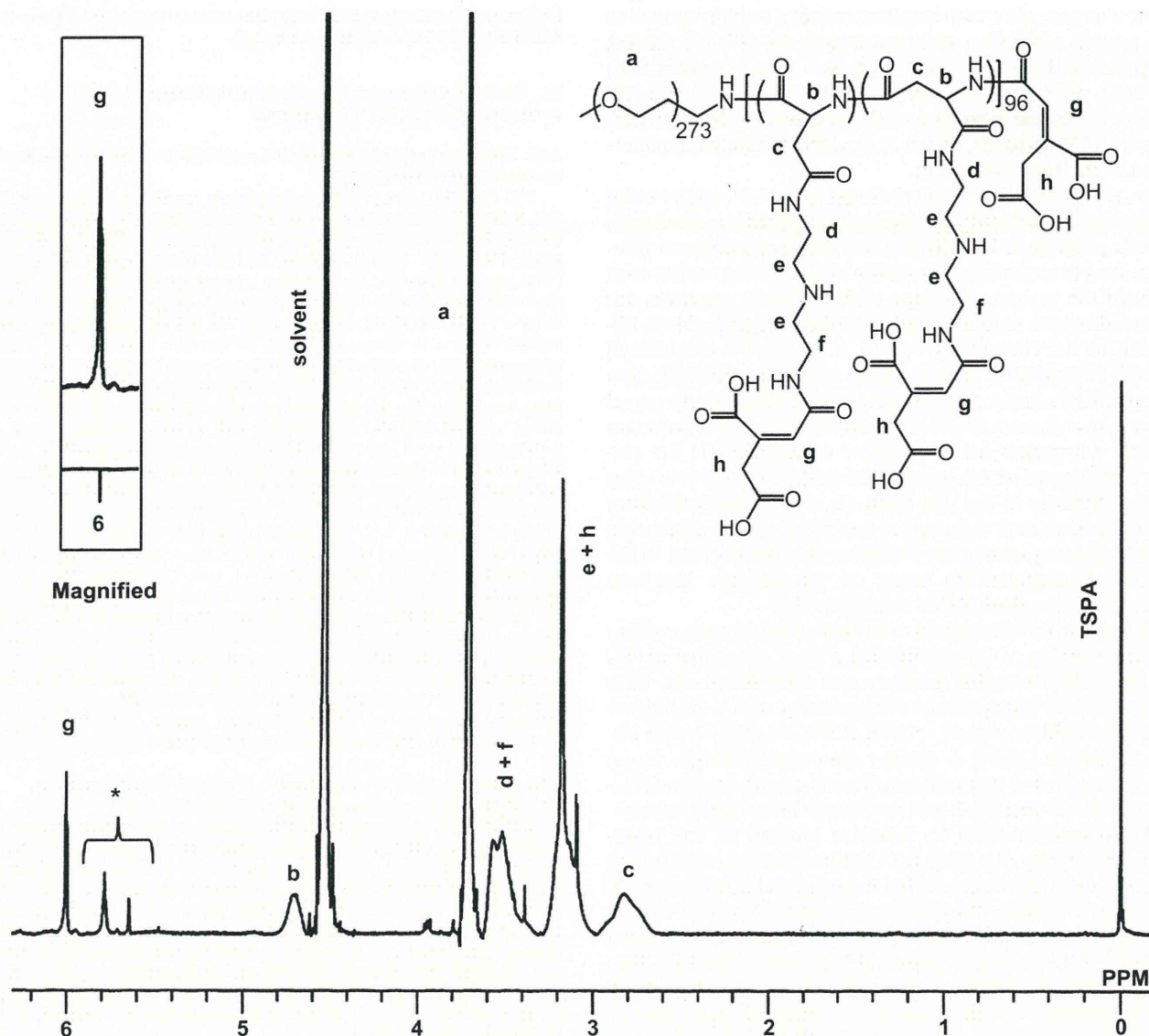


**Fig. 1.**  $^1\text{H}$  NMR spectrum of the synthesized PEG-polyanion block copolymer, PEG-PAsp(DET-Aco) (Concentration: 10 mg/mL, Solvent:  $\text{D}_2\text{O}$ , Temperature: 50 °C). \*Decarboxylated itaconitylamide (Supporting Information).

### 2.3.3. Synthesis of poly(ethylene glycol)-*b*-poly(aspartic acid) (PEG-PAsp)

PEG-PBLA (20 mg, 0.06 mmol) was dissolved in acetonitrile (1.5 mL). Aqueous sodium hydroxide (0.5 N, 6 mL, 50 equiv to benzyl group of PBLA segment) was added to the first solution and allowed to react for 1 h stirring at room temperature. The solution was dialyzed against de-ionized water. A white powder was obtained after lyophilization of the dialyzed solution (18.2 mg, 93.0% yield). The complete deprotection of the flanking benzyl esters in PBLA was confirmed by the peak disappearance of benzyl protons of PBLA ( $-\text{CH}_2\text{C}_6\text{H}_5$ ,  $\delta = 7.3$ ) in the  $^1\text{H}$  NMR spectrum in  $\text{D}_2\text{O}$  at 50 °C (data not shown).

### 2.4. Preparation of PEG-polyanion/siRNA/CaP hybrid nanoparticles

A solution of 2.5 M  $\text{CaCl}_2$  was diluted in 10 mM Tris/HCl buffer (pH 7.5) (1  $\mu\text{L}$ : 11.5  $\mu\text{L}$ ). Another solution containing PEG-PAsp(DET-Aco) or PEG-PAsp(DET-Car) (1000  $\mu\text{g}/\text{mL}$ ) in 10 mM Tris/HCl buffer (pH 7.5) was mixed with a solution of 15  $\mu\text{M}$  siRNA in 10 mM Hepes buffer (pH 7.2) and with 50 mM Hepes buffer containing 1.5 mM  $\text{Na}_3\text{PO}_4$  and 140 mM NaCl (pH 7.5) (2.5  $\mu\text{L}$ : 5  $\mu\text{L}$ : 5  $\mu\text{L}$ ). The former solution was mixed with the latter solution by pipetting for around 20 s (final siRNA concentration; 3  $\mu\text{M}$ ). A control nanoparticle containing PEG-PAsp was built as previously described [9]. Each sample solution was used immediately after preparation.

### 2.5. Dynamic light scattering (DLS)

For the determination of size distribution of hybrid nanoparticles, DLS measurements were carried out at 25 °C using a Zetasizer Nano ZS (Malvern Instruments, UK) at a detection angle of 173° with a He-Ne laser (633 nm) as the incident beam. The data

obtained from the rate of decay in the photon correlation function were analyzed with a cumulant method to obtain the corresponding hydrodynamic diameters and polydispersity indices (Pdl) ( $\mu/\Gamma^2$ ) of the nanoparticles.

### 2.6. Determination of siRNA encapsulated in hybrid nanoparticle

The assay to estimate the amount of siRNA encapsulated in hybrid nanoparticles was carried out as previously reported [11]. Briefly, the sample solutions were centrifuged at 15,000g for 30 min to precipitate the nanoparticles. The supernatant was carefully collected to determine the siRNA concentration by measurement of absorbance at 260 nm ( $\text{Abs}_{260}$ ). The percentage of the loaded siRNA was calculated as follows;

$$\text{Encapsulated percentage (\%)} = 100 - (\text{Abs}_{260} \text{ after centrifuge}) / (\text{Abs}_{260} \text{ before centrifuge}) \times 100$$

### 2.7. Transmission electron microscopy (TEM) observation

TEM observation was conducted using H-7000 electron microscope (Hitachi, Tokyo, Japan) operated at 75 kV acceleration voltages. Copper TEM grids with carbon-coated collodion film were glow-discharged for 20 s using an Eiko IB-3 ion coater (Eiko Engineering Co. Ltd., Japan). The grids were dipped into complex solution with 3  $\mu\text{M}$  siRNA, which was mixed with uranyl acetate solution (2% (w/v)), for 30 s. After excess solution was removed using a filter paper, the sample grids were allowed to dry in air and then TEM observation was carried out.

## 2.8. Cell viability assay

For the cytotoxicity assay, PanC-1 cells (Pancreatic cancer cells, ATCC Number: CRL-1469) were seeded with 100  $\mu$ L of DMEM containing 10% FBS in a 96 well plate (5000 cells/well) and incubated for 24 h. The nanoparticles (containing 10–1500 nm siRNA) were added with the fresh medium containing 10% FBS, and the cell viability was evaluated after 48-h incubation by Cell Counting Kit-8 (Dojindo, Kumamoto, Japan) according to the protocol provided by the manufacturer. Each well was measured by reading the absorbance at 450 nm in a Microplate Reader (Bio-Rad Model 680, Bio-Rad Laboratories, UK). The results were expressed as the percentage (%) of the control cells, which were incubated only with the culture medium.

## 2.9. Confocal laser scanning microscopy (CLSM) observation

PanC-1 cells were cultured with 1.5 mL of DMEM containing 10% FBS on 35-mm glass-base dishes (Iwaki, Japan) at  $5 \times 10^4$  cells/dish. After 24 h, the medium was exchanged with fresh one and Cy5-labeled siRNA-containing nanoparticles were applied to the dish (100 nm siRNA). The nuclei and the endosome/lysosome were stained with Hoechst 33342 (Dojindo Laboratories, Kumamoto, Japan) for 5 min and LysoTracker Green (Molecular Probes, Eugene, OR) for 15 min before CLSM imaging, respectively. Cells were rinsed 3 times with PBS and fresh medium was added prior to the imaging. CLSM images were acquired at 3 and 24 h after nanoparticle administration, using a Zeiss LSM 510 META (Carl Zeiss, Germany) with a water-immersion 63 $\times$  objective (C-Apochromat, Carl Zeiss). Excitation wavelengths were 488 nm (argon laser), 633 nm (He–Ne laser), and 710 nm (Mai Tai laser, operated in a two-photon mode) for LysoTracker, Cy5, and Hoechst 33342, respectively. The co-localization ratio was calculated as previously described [24] with the formula:

Co-localization ratio = number of yellow pixels/number of yellow and red pixels.

## 2.10. Real-time reverse transcription (RT)-PCR

PanC-1 cells were seeded with 2000  $\mu$ L of DMEM containing 10% FBS on a 6 well plate at  $8 \times 10^4$  cells/well. After 24 h, nanoparticles were added with fresh medium (60 nm siRNA). After 3 h of exposing the cells to nanoparticles, the medium was changed to fresh one. Twenty four hours later, cells were harvested and RNA was extracted using the RNeasy Mini Kit (Qiagen, Valencia, CA), according to the

manufacturer's instruction. The amount of extracted RNA was measured and standardized after the genomic DNA elimination for the cDNA synthesis (QuantiTect Reverse Transcription, Qiagen, Valencia, CA). Real-time RT-PCR was performed using the ABI 7500 Fast Real-time RT-PCR System (Applied Biosystems, Foster City, CA) and QuantiTect SYBR Green PCR Master Mix (Qiagen, Valencia, CA). The actin was used as a house-keeper gene and the obtained data were normalized before statistical analysis.

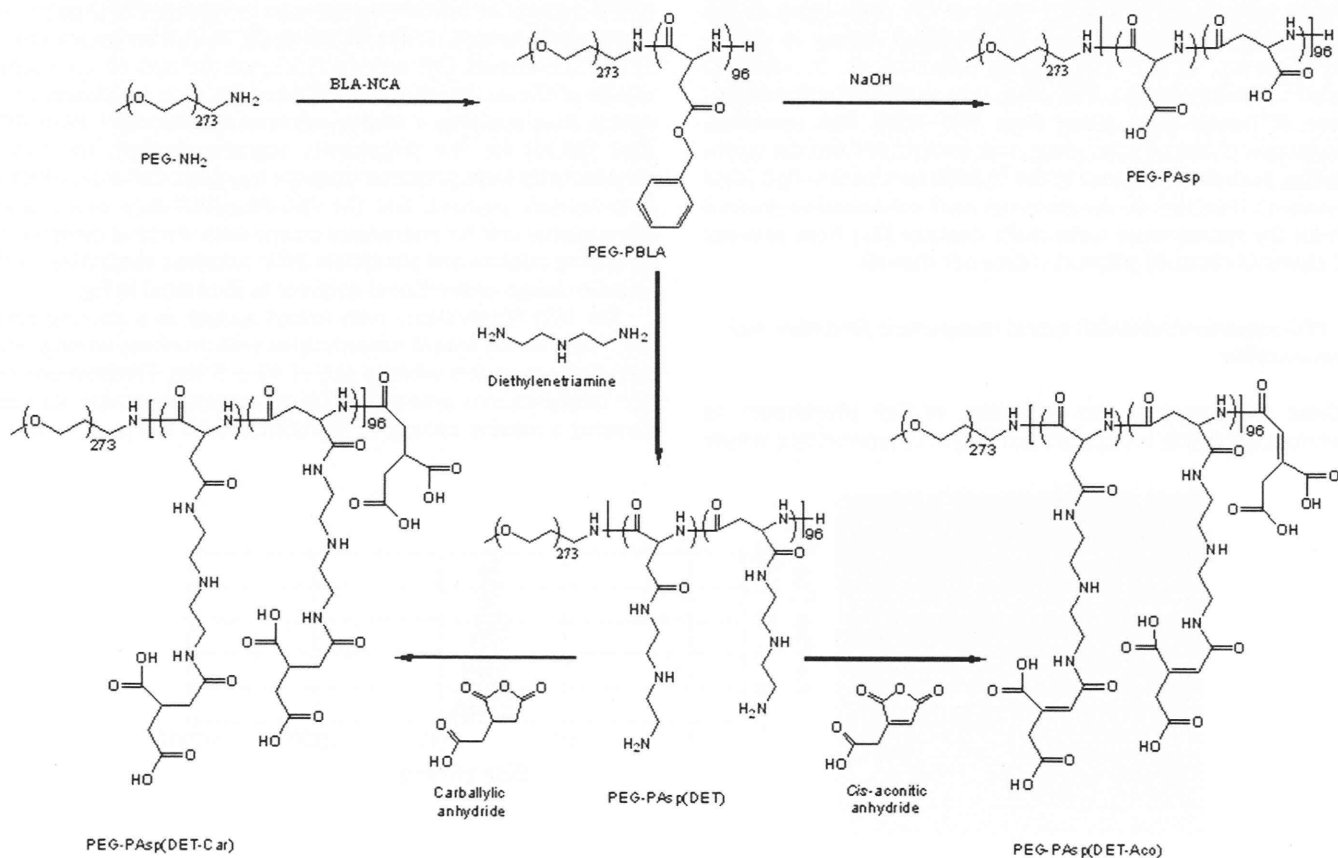
## 2.11. Statistical analysis

The analysis of variance (ANOVA) was performed to test the treatment effects, and Bonferroni's test was used as *post hoc* pairwise comparisons between individual treatment groups, using the software GraphPad Prisma 3.0 (GraphPad Software, Inc.). Statistical significance is represented as \* for  $p < 0.05$  and \*\* for  $p < 0.01$ . Unless indicated, all experiments were performed in triplicate ( $N = 3$ ) and the results reported were expressed as mean values ( $\pm$ SEM).

## 3. Results and discussion

### 3.1. Synthesis of charge-conversional and non-charge-conversional polymers

The synthesis route of PEG-PAsp(DET-Aco) as a charge-conversional polyanion is illustrated in Scheme 1, as well as two polyanions used as controls without the charge-conversional property. PEG-PAsp(DET) was synthesized from PEG–PBLA ( $M_w$  of PEG 12,000; DP of PBLA 96) by aminolysis reaction with excess of DET molecules. The  $^1\text{H}$  NMR measurement revealed the quantitative introduction of the *N*-(2-aminoethyl)-2-aminoethyl moiety for successful synthesis of PEG-PAsp(DET) (data not shown). Further, the *cis*-aconityl moiety (Aco) was introduced into the primary amine in the side chain of PAsp(DET) by reacting *cis*-aconitic anhydride with PEG-PAsp(DET) to form an acid-labile *cis*-aconitylamide in the side chain. The quantitative conversion of primary



Scheme 1. Synthetic routes of PEG-PAsp(DET-Aco), PEG-PAsp(DET-Car), and PEG-PAsp.

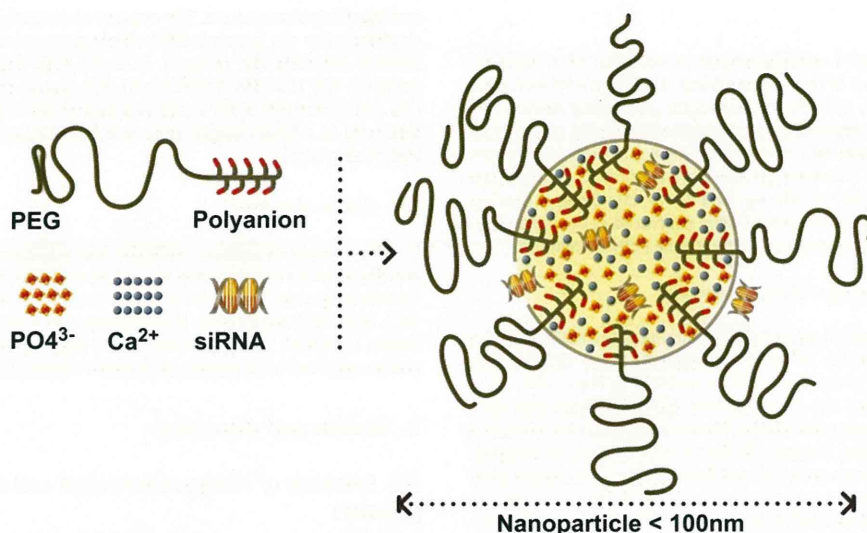


Fig. 2. Schematic illustration of PEG-polyanion/siRNA/CaP hybrid nanoparticles.

amines in Asp(DET) side chain to *cis*-aconitylamide was confirmed from the peak intensity ratio of the methine protons in the main chain to methine protons of the *cis*-aconityl moiety in the  $^1\text{H}$  NMR spectrum in  $\text{D}_2\text{O}$  (Fig. 1). Although it was also possible to observe the formation of reaction subproducts [27], the desired product of PEG-PAsp(DET-Aco) was obtained in a high ratio (80%). PEG-PAsp(DET-Car) without the acid-labile bond as a control was synthesized by reacting PEG-PAsp(DET) with carballylic anhydride similarly. The quantitative conversion of the primary amines in the Asp(DET) side chain to carballylylamide was confirmed from the peak intensity ratio of the methine protons in the main chain to the methine and methylene protons of carballylyl moiety in the  $^1\text{H}$  NMR spectrum in  $\text{D}_2\text{O}$  (Supporting Information). In addition, another control polyanion, PEG-PAsp, was prepared by the deprotection of benzyl ester group from PEG-PBLA. The successful deprotection of benzyl ester group was confirmed from the corresponding peak disappearance in the  $^1\text{H}$  NMR spectrum in  $\text{D}_2\text{O}$  (data not shown). Note that all the reactions were confirmed to proceed without the spontaneous main-chain cleavage [21] from aqueous GPC charts of obtained polymers (data not shown).

### 3.2. PEG-polyanion/siRNA/CaP hybrid nanoparticle formation and characterization

Great advantages in the utilization of CaP precipitates as a transfection reagent are the fact that they are prepared by a simple

and inexpensive method, and also that it efficiently binds/encapsulates polyanions/nucleic acids during the formation process [28,29]. Through self-assembly, CaP nanoparticles containing nucleic acid are formed by the precipitation method in which calcium chloride and phosphate solutions are mixed in the presence of siRNA. However, simple CaP precipitates have potential problems to overcome for efficient nucleic acids delivery; one is the increase in size with time to form large agglomerates in aqueous solutions, and another is poor endosomal escape. To prevent the size increase in CaP precipitates, our previous studies have addressed a preparation of PEG-coated CaP hybrid nanoparticles by mixing of PEG-polyanion block copolymers [9,11–14]. In this study, for further improvement of the PEG-coated CaP nanoparticles, we focused on endosomal escape of the nanoparticles to enhance the gene knockdown efficiency, thus applying a charge-conversional structure PAsp(DET-Aco) [23,24] for the polyanionic segment. Indeed, the hybrid nanoparticles were prepared from the inorganic CaP core, siRNA as a therapeutic payload, and the PEG-PAsp(DET-Aco) as a charge-conversional unit for endosomal escape with minimal cytotoxicity, by mixing calcium and phosphate ionic solutions containing siRNA and the charge-conversional polymer as illustrated in Fig. 2.

The TEM observations with uranyl acetate as a staining agent (Fig. 3A) revealed hybrid nanoparticles with relatively homogenous spherical shape and average size of  $42 \pm 5$  nm. Furthermore, the DLS measurements provided a size histogram in number statistics showing a narrow unimodal distribution with the peak at 38 nm

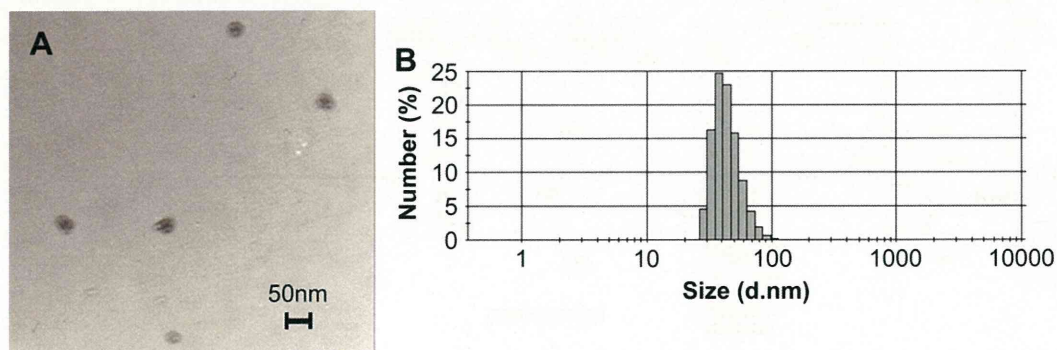
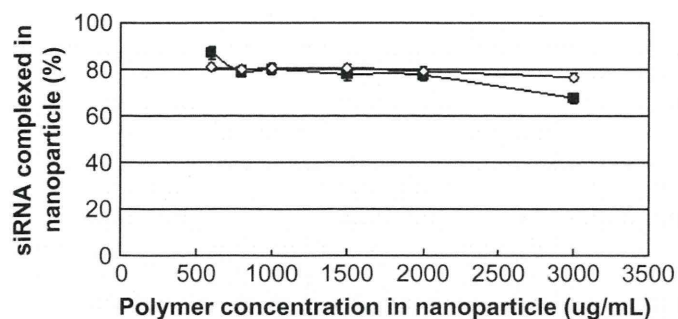


Fig. 3. Size and morphology of PEG-PAsp(DET-Aco)/siRNA/CaP hybrid nanoparticles. A: TEM image (Scale Bar: 50 nm). B: Histogram in number statistics determined by DLS measurement (1 mg/mL PEG-PAsp(DET-Aco) and  $3 \mu\text{M}$  siRNA).



**Fig. 4.** Percentage of siRNA loaded by the hybrid nanoparticle at varying polymer concentrations (3  $\mu$ M siRNA). Closed square: PEG-PAsp(DET-Aco), Open diamond: PEG-PAsp(DET-Car).

(Fig. 3B), which was well correlated to the size determined by the TEM observations (Fig. 3A). Samples were confirmed to have the same size even after prolonged incubation time. These results indicate that hybrid nanoparticles can be obtained in a controllable manner using the charge-conversional polymer as colloidal stability agent.

The amount of siRNA encapsulated in the hybrid nanoparticles was monitored against polyanion concentration, determined by the centrifugal assay as previously reported [11]. Effective encapsulation of siRNA in the nanoparticles (around 80%) was confirmed in PEG-PAsp(DET-Aco) concentration between 600 and 2000  $\mu$ g/mL, while a slight decrease was observed at the concentration of 3000  $\mu$ g/mL (around 70%) (Fig. 4). Note that the similar binding tendency was observed for the nanoparticle from PEG-PAsp(DET-Car). The siRNA-loading capacities obtained here were close to those found in our previous work with PEG-PAsp (around 85%) [11], indicating efficient entrapment of siRNA by this method regardless of polyanion structures.

### 3.3. Gene knockdown and cell viability assays

The development of an effective and non-cytotoxic carrier is the main challenge to the success in RNAi therapy. We verified the gene

knockdown efficiency of the hybrid nanoparticles to a cultured pancreatic cancer cell (PanC-1) by measuring the level of mRNA. Here, vascular endothelial growth factor (VEGF) was chosen as a target gene because many cancer cells up-regulate VEGF expression to promote angiogenesis, a process characterized by the formation of new blood vessels from a pre-existing vascular network [30,31], facilitating the tumor growth and proliferation. Hence, VEGF knockdown in such cancer cells with siRNA *in vivo* is expected to be a promising strategy to suppress the tumor growth and control cancer evolution (anti-angiogenic therapy).

Hybrid nanoparticles containing 60 nm siVEGF or siLuc as a non-targeted control sequence were applied to PanC-1 cells, and after 3 h of exposure time the medium was replaced and cells were further incubated for 24 h. Thereafter, the real-time RT-PCR analysis was used to determine the mRNA for VEGF. The results revealed that all the tested hybrid nanoparticles with siVEGF possessed potential gene knockdown activity, whereas the nanoparticles with siLuc and naked siVEGF showed no gene knockdown (Fig. 5), indicating the siVEGF sequence-specific gene knockdown with the hybrid nanoparticles. Among them, the nanoparticle from PEG-PAsp(DET-Aco) presented the only significant and highest gene knockdown (~82%). The comparison of PEG-PAsp(DET-Aco) with the other PEG-polyanions strongly suggests that the acid-labile *cis*-aconitylamide in PEG-PAsp(DET-Aco) should be essential for the significant gene knockdown. Next, the cytotoxicity of the hybrid nanoparticles was evaluated to PanC-1 cells. A wide range of siRNA concentration was tested from 10 to 1500 nM along with the increase in all the other components. As shown in Fig. 6, no significant cytotoxicity was observed for both hybrid nanoparticles from PEG-PAsp(DET-Aco/Car) even at the highest concentration (50  $\mu$ g/mL PEG-polyanion, 1.5  $\mu$ M siRNA). From these results, we concluded that the hybrid nanoparticles from PEG-PAsp(DET-Aco) allowed efficient siRNA delivery into the cytoplasm of cultured PanC-1 with negligible cytotoxicity.

### 3.4. Cellular uptake and intracellular trafficking

In siRNA transfection process, after cellular internalization as the first hurdle, siRNA carriers will be delivered to early endosomes,

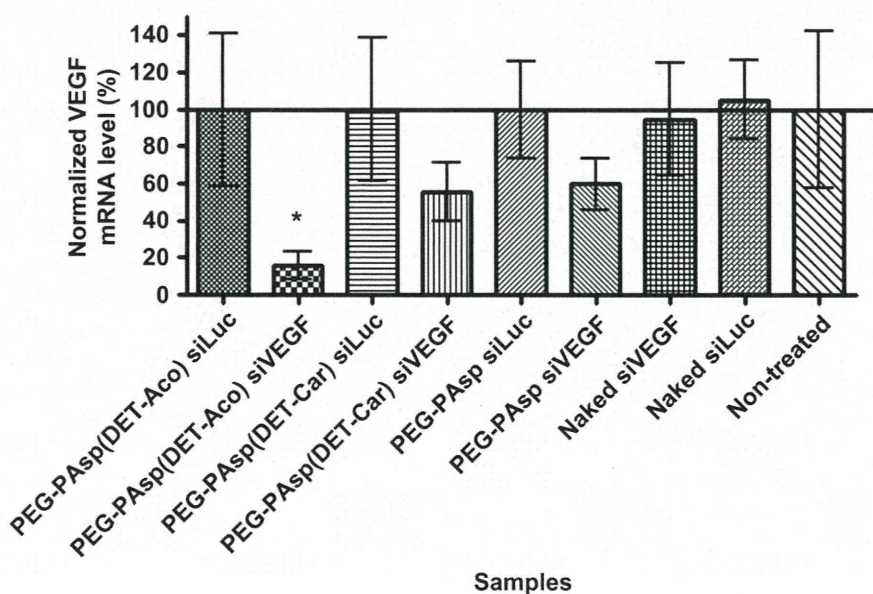


**Fig. 5.** Gene knockdown in PanC-1 at 24 h after 3 h of nanoparticles exposition to cells (60 nm siRNA, N = 9). Controls were set as 100%. \* $p < 0.05$  comparing to controls (ANOVA followed by Bonferroni).